Biochemical characterisation of the Mycobacterium tuberculosis phosphoribosyl-1-pyrophosphate synthetase (Mt-PrsA).

Alderwick, Luke; Lloyd, Georgina; Lloyd, Adrian; Lovering, Andrew; Eggeling, L; Besra, Gurdyal

DOI:
10.1093/glycob/cwq173

Glycobiology Advance Access published November 2, 2010

Biochemical characterisation of the *Mycobacterium tuberculosis* phosphoribosyl-1-pyrophosphate synthetase (Mt-PrsA)

Luke J. Alderwick[1], Georgina S. Lloyd[1], Adrian J. Lloyd[2], Andrew L. Lovering[1], Lothar Eggeling[3], and Gurdyal S. Besra[1,4]

[1]School of Biosciences, University of Birmingham, Edgbaston Park Road, Birmingham, B15 2TT, UK; [2]Department of Biological Sciences, University of Warwick, Coventry, CV4 7AL, UK; [3]Institute of Biotechnology 1, Forschungszentrum Julich GmbH, D-52425 Julich, Germany

[4]To whom correspondence should be addressed: Mailing address: School of Biosciences, University of Birmingham, Edgbaston, Birmingham B15 2TT, United Kingdom. Phone: 44 121 415 8125. Fax: 44 121 414 5925. E-mail: g.besra@bham.ac.uk

Abstract

Mycobacterium tuberculosis arabinogalactan (AG) is an essential cell wall component. It provides a molecular framework serving to connect peptidoglycan to the outer mycolic acid layer. The biosynthesis of the arabinan domains of AG and lipoarabinomannan (LAM), occurs *via* a combination of membrane bound arabinofuranosyltransferases, all of which utilise decaprenol-1-monophosphorabinose as a substrate (DPA). The source of arabinose ultimately destined for deposition into cell wall AG or LAM, originates exclusively from phosphoribosyl-1-pyrophosphate (pRpp), a central metabolite which is also required for other essential metabolic processes, such as *de novo* purine and pyrimidne biosynthesis. In *M. tuberculosis*, a single pRpp synthetase enzyme (Mt-PrsA) is soley responsible for the generation of pRpp, by catalysing the transfer of pyrophosphate from ATP to the C1 hydroxyl position of ribose-5-phosphate. Here, we report a detailed biochemical and biophysical study of Mt-PrsA, which exhibits the most rapid enzyme kinetics reported for a pRpp synthetase.

Key words: Mycobacteria/ cell wall/ polysaccharides/ arabinan/ phosphoribosylpyrophosphate

Introduction

As we enter into the second decade of the twenty first century, tuberculosis (TB) continues to cause more deaths and human suffering than any other infectious disease (Dye, 2006). The number of new TB cases is increasing at an alarming pace, as does the prevalence of drug resistant stains of the causative agent, *Myobacterium tuberculosis*, in the form of multidrug-resistant TB (MDR-TB) and extensively drug resistant TB (XDR-TB) (Madariaga *et al.*, 2008). The need for new drugs and vaccines to combat this major burden to human health is overwhelming.

The unique hydrophobic cell wall of *M. tuberculosis* forms a primary defensive barrier to the onslaught of toxic insult during the host immune response. The current chemotherapeutic regime used to treat TB includes the administration of isoniazid and ethambutol, both of which target crucial steps in the biosynthesis and assembly of the *M. tuberculosis* cell wall (Banerjee *et al.*, 1994; Belanger *et al.*, 1996). However, whilst these cell wall inhibitors are excellent at effectively killing actively dividing cells, certain sub-populations of bacilli, labelled as ‘persisters’, exhibit transient resistance to many of the drugs used to treat TB (Wayne & Sohaskey, 2001). The precise molecular mechanism of this latent infection caused by persistent bacilli is poorly understood. However, in the pursuit of identifying suitable cellular targets and the development of new anti-TB chemotherapeutic agents, we must address the phenomenon of persistence to truly eradicate the disease. Recently it has been shown that certain processes of metabolic pathways involved in mycobacterial cellular energy metabolism, such as respiratory ATP biosynthesis, represent excellent physiological targets for the effective killing of latent

populations of TB bacilli (Bald & Koul, 2010; Koul *et al.*, 2007; Koul *et al.*, 2008). Phospho-α-D-ribosyl-1-pyrophosphate (pRpp) is a central metabolite that links the pentose phosphate pathway to the *de novo* and salvage biosynthetic pathways of purine and pyrimidine production, NAD and NADP cofactor biosynthesis, as well as histidine and tryptophan biosynthesis (Hove-Jensen, 1988). It is therefore considered that pRpp is required at all times during the life cycle of both prokaryotic and eukaryotic cells (Hove-Jensen, 1989; Tozzi *et al.*, 2006). In addition to these central metabolic processes described above, members belonging to the *Corynebacteriacae*, such as mycobacteria, have evolved an almost unique biochemical pathway, utilising pRpp as a high-energy biosynthetic precursor for cell wall arabinan biosynthesis (Scherman *et al.*, 1995; Scherman *et al.*, 1996; Wojtkiewicz *et al.*, 1988) (Fig. 1). The gene product of *Rv3806c* encodes for a membrane bound pRpp:decaprenol-1-monophosphate 5-phosphoribosyltransferase (DPPR synthase) which catalyses the formation of decaprenol-1-monophosphoribose-5-phosphate (DPPR) and pyrophosphate from pRpp and decaprenol-1-monophosphate (Huang *et al.*, 2005). DPPR then undergoes C5-dephosphorylation to decaprenol-1-monophosphoribose (DPR) and epimerisation about the C2-OH position of the ribosyl moiety catalysed by a two-step heteromeric oxidation/reduction process (Mikusova *et al.*, 2005). In *M. tuberculosis*, Rv3790 encodes for a FAD-containing oxidoreductase (DprE1) which oxidises the ribosyl C2-OH group to the keto sugar decaprenol-1-monophosphoryl-2-keto-β-*erythro*-pentofuranose (DPX) which is subsequently reduced by DprE2 (encoded by Rv3791) forming decaprenol-1-monophosphoarabinose (DPA) (Mikusova *et al.*, 2005), which is the sole high-energy

lipid linked substrate for the GT-C family arabinofuranosyltransferases (AraTs) which are involved in cell wall arabinan polymerisation (Alderwick *et al.*, 2007).

Mycobacterial arabinan is a highly branched polysaccharide consisting of arabinose units arranged into specific repeating motifs, and it predominantly features in the heteropolysaccharide arabinogalactan (AG), which is a crucial component of the mycobacterial cell wall (Besra *et al.*, 1995; Daffé *et al.*, 1990). Three arabinan domains are covalently linked *via* an Ara*f*-α(1→5)-Gal*f* glycosidic bond to the 8th, 10th and 12th positions of a single linear polysaccharide composed of ~30 alternating β(1→5) and β(1→6) Gal*f* residues forming the galactan domain of AG (Alderwick *et al.*, 2005). AG is a structural macromolecule and serves to function as a molecular scaffold linking peptidoglycan (PG) to the mycolic acids, forming a highly impermeable and hydrophobic layer surrounding the mycobacterial cell (McNeil *et al.*, 1991). Arabinan is also present in the form of lipoarabinomannan (LAM), a highly immunogenic lipoglycan, which is involved in modulating the host immune response (Briken *et al.*, 2004). In terms of chemical composition, arabinan represents approximately 18% of mycobacterial cell wall biomass (Ortalo-Magne *et al.*, 1995). Therefore, during cell elongation and division of the mycobacterial bacilli, it is necessary for there to be a readily available supply of pRpp for the efficient incorporation of arabinose into newly synthesised cell wall material. During this process, the metabolic demand for pRpp is likely to increase dramatically and the elevated levels required for effective arabinan biosynthesis must be maintained. The enzyme pRpp synthetase (ATP: α-D-ribose-5-phosphate pyrophosphotransferase; EC2.7.6.1) belongs to a family of enzymes that catalyse the transfer of the β,γ-

diphosphate moiety from ATP to the C1-OH group of α-D-ribose-5-phosphate (R5P) and the gene(s) encoding for this enzyme(s) is present in all living organisms (Carter *et al.*, 1997; Hove-Jensen, 1985; Krath & Hove-Jensen, 1999). It is predicted that the *M. tuberculosis* H37Rv genome codes for only one pRpp synthetase (*Rv1017c*), which is annotated as Mt-PrsA (Cole & Barrell, 1998).

In this study, we report a detailed biochemical characterisation of recombinant Mt-PrsA and provide evidence which confirms the essentiality of this gene for the maintenance of cell growth, division and integrity. Mt-PrsA displays an absolute requirement for inorganic phosphate for enzyme activation and will accept either Mg^{2+} or Mn^{2+} as divalent cations, which serve to coordinate the phosphate moieties of ATP during enzyme catalysis. Using a continuous enzyme coupled spectrophotometric assay, we report a detailed kinetic characterisation of Mt-PrsA, which displays the highest specific activity measured for any a pRpp synthetase studied to date. By investigating the oligomeric state of Mt-PrsA in solution and measuring the ligand binding properties of its substrates, we provide evidence suggesting that the mechanism by which ADP inhibits Mt-PrsA activity, results from the binding of ADP to an allosteric site, and as a consequence, induces the stabilisation of an inactive, hexameric oligimeric species.

Results

Evidence suggesting that *Mt-prsA* is an essential gene for the maintenance of cellular integrity

Mt-prsA is predicted to be an essential gene as determined by high density transposon mutagenesis (Sassetti *et al.*, 2003). This is not unsurprising, considering the apparent physiological importance of Mt-PrsA in the provision of pRpp for central metabolic pathways and the formation of the cell wall biosynthetic precursor DPA (Scherman *et al.*, 1995; Wolucka *et al.*, 1994). We have previously used *Corynebacterium glutamicum* as an excellent model system for the study of complex cell wall biosynthetic processes, and we have reported the phenotypic characterisation of several cell wall mutants, which would otherwise be essential in mycobacterial systems (Alderwick *et al.*, 2005; Alderwick *et al.*, 2006a; Alderwick *et al.*, 2006b; Birch *et al.*, 2008; Gande *et al.*, 2004; Seidel *et al.*, 2007). A bioinformatics analysis of several *Corynebacteriaceae* genomes revealed that *NCgl0945* (*Cg-prsA*) was the likely *C. glutamicum* ortholog of *Mt-prsA* (*Rv1017c*). These corresponding gene products share 71% identity (83% similarity) and the gene locus is conserved within the *Corynebacteriaceae* indicating that this region is syntenic. We attempted to inactivate *Cg-prsA* in *C. glutamicum*, by using the disruption vector pK18mob-*Cg-prsA*-int, carrying 304 bp of *Cg-prsA*. In a control experiment, we used the previously reported pK18mob-*Cg-ppm1*-int construct, which affords the successful inactivation of the gene encoding for the polyprenyl monophosphomannose synthase (*ppm1*) of *C. glutamicum*, which is a gene of similar size to that of *Cg-prsA* (Gibson *et al.*, 2003). Both inactivation vectors were used in parallel experiments for the transformation of wild type (WT) *C. glutamicum* to kanamycin resistance (Kan^R). Whilst we were able to easily generate *C. glutamicum* Kan^R colonies from the pK18mob-*Cg-ppm1*-int construct, we were required to conduct several rounds of electroporation using pK18mob-*Cg-prsA*-int before obtaining three separate *C. glutamicum* Kan^R clones. This

indicates that the recombination events appeared to have taken place at unexpected and, as yet, undefined loci. From this analysis, we concluded that *Cg-prsA* is an essential gene and its function is necessary for the growth and integrity of *C. glutamicum*, even when grown on rich Brain Heart Infusion (BHI) medium.

Over-expression, purification and pRpp synthetase activity of recombinant Mt-PrsA

Over-expression of Mt-PrsA in *Escherica coli* C41 cells and the subsequent purification by IMAC, resulted in a preparation of Mt-PrsA that was stable in solution at a concentration of 2 mg/ml. A coomassie-stained 12 % SDS-PAGE analysis of Mt-PrsA revealed a band that migrated to a position of 35 kDa, which is in accordance with the expected molecular weight of Mt-PrsA and was estimated to be at least 98% pure. To determine if recombinant Mt-PrsA was active, we performed a radiochemical assay to measure the pyrophosphate transfer from ATP to the C1-OH group of [^{14}C]-uniformly labelled R5P (Boss *et al.*, 1984). Starting with [^{14}C]-U-D-glucose, and replicating the first three enzymic reactions of the pentose phosphate pathway *in vitro* using commercially available enzymes (Roche and Sigma), we prepared a source of purified [^{14}C]-U-α-D-ribose-5-phosphate as a substrate for subsequent enzyme assays. In a time course assay, recombinant Mt-PrsA exhibited rapid pRpp synthetase activity which was dependent upon the presence of either of the divalent cations Mg^{2+} and Mn^{2+}, with slight preference for the latter (Fig. 2a). During the assay, p[^{14}C]Rpp is susceptible to product degradation due to hydrolysis of the labile C1-OH pyrophosphate bond, which accounts for the relatively small increase in band density (relating to p[^{14}C]Rpp) over the course of the assay. Addition of EDTA to the reaction mix inhibited the formation of p[^{14}C]Rpp (data

not shown) and the inclusion of $CaCl_2$, in replacement of $MgCl_2$ or $MnCl_2$, also resulted in loss of Mt-PrsA activity (Fig 2a). Mt-PrsA was found to be most active at a pH of 6.5, but also showed activity across a broad range of pH levels (4.5 – 9.5) and was only found to be inactive at high pH (10.5) (data not shown). In accordance with previous studies of pRpp synthetases (Prs) from other organisms, Mt-PrsA was strongly inhibited by the presence of ADP, which has been shown to be an allosteric modulator of this class of enzymes (Fig. 2b) (Arnvig *et al.*, 1990; Eriksen *et al.*, 2000; Gibson *et al.*, 1982; Switzer & Sogin, 1973; Willemoes *et al.*, 2000).

Mt-PrsA-dependent metabolic channelling of R5P into mycobacterial cell wall biosynthetic precursors

Apart from being a key metabolite in the *de novo* and salvage pathways of purine and pyrimidine biosynthesis, as well as histidine, tryptophan, NAD and NADP metabolism, pRpp serves as a high-energy intermediate in the formation of the mycobacterial cell wall precursor DPR (Fig. 1) (Scherman *et al.*, 1995). We investigated the conversion of [^{14}C]-R5P into the cell wall AraT substrate DPA and its precursor, DPR. Assays were conducted using membranes prepared from *M. smegmatis* which provided a source of DPPR synthase (Huang *et al.*, 2005), which was necessary to investigate incorporation of [^{14}C]-R5P into lipid-linked organic extractable material. When assays were performed with just [^{14}C]-R5P and membranes, no radioactive product was detectable in the organic phase, as depicted in Figure 3, lane 1. In this instance, all radioactivity remained in the aqueous phase of the assay work-up (data not shown). In addition, *M. smegmatis* P60 (a preparation of cell wall material rich in proteins associated with cell wall processes)

exhibited no pRpp synthetase activity (Fig. 3, lane 2). When recombinant Mt-PrsA is included in the assay, the formation of DPPR and DPR can be clearly observed (Fig. 3, lane 3). It is likely that DPPR undergoes enzyme catalysed 5'-dephosphorylation, resulting in the formation of DPR. In *M. tuberculosis*, Rv3807c is an excellent candidate for this enzyme since it codes for a putative membrane bound PAP2 phosphatase directly adjacent to the DPPR synthase (Rv3806c) (Fig. 1) (Cole & Barrell, 1998). *M. smegmatis* has a direct orthologue of this phosphatase encoded by *MSMEG6402*, which explains the apparent conversion of DPPR to DPR observed in this assay. The combined addition of sodium fluoride and sodium tungstate (known phosphatase inhibitors (Stankiewicz & Gresser, 1988)) to the assay mix, results in a diminished level of DPR formation and a corresponding increase in a band migrating to a lower position on the TLC identified as being DPPR (Fig. 3 lane 4). When Mt-PrsA is used in combination with *M. smegmatis* P60, two additional bands can be observed migrating in close proximity to DPR, which correspond to the subsequent conversion of DPR to DPX and DPA, by the endogenous P60 activity of DprE1 and DrpE2, respectively (Fig. 3, lane 5) (Mikusova *et al.*, 2005). Inclusion of sodium fluoride and sodium tungstate dramatically reduced the conversion of DPPR to DPA, suggesting that the two-step epimerisation of the C2-OH group of ribose by DprE1 and DprE2 occurs after 5' dephosphorylation (Fig. 3, lane 6). The inclusion of ADP to the reaction mix completely ablated the formation of any organic extractable material, clearly indicating that ADP inhibition of Mt-PrsA results in the total loss of DPPR formation (Fig. 3, lane 7).

In a separate experiment, assays were carried out in the presence of a neo-glycolipid acceptor [Ara*f*-α(1→5)-Ara*f*-*O*-(CH_2)CH_3], which is specific for measuring the activity of the cell wall biosynthetic arabinofuranosyltransferases EmbA, EmbB, EmbC and AftB (Lee *et al.*, 1997; Seidel *et al.*, 2007), all of which reside in the membrane due to the polytopic nature of these GT-C family glycosyltransferases. AraT activity was measured after product isolation by organic extraction and analysis by TLC and autoradiography. AraT assays carried out in the absence of Mt-PrsA afforded no AraT-dependent product formation (Fig. 4, lane 1). Upon addition of Mt-PrsA, two closely migrating bands could be observed with the top bad attributed to α(1→5)-Ara*f* transfer to the acceptor by either EmbA, EmbB, EmbC (or a combination) and the lower band attributed to β(1→2)-Ara*f* transfer resulting from AftB activity (Fig. 4, lane 2), as previously described (Lee *et al.*, 1997). Addition of the EmbA, EmbB and EmbC inhibitor ethambutol (EMB), resulted in the loss of the upper band with only the lower band remaining, this being due to the non-inhibitory effect of EMB on the terminal β(1→2) capping enzyme, AftB (Seidel *et al.*, 2007) (Fig. 4, lane 3). As a consequence of allosteric inhibition of Mt-PrsA and the resultant loss of *in vitro* Mt-PrsA-dependent pRpp formation, the inclusion of ADP in the assay mixture led to inhibition of any AraT-dependent product formation (Fig. 4, lane 4).

Kinetic characterisation of Mt-PrsA substrates and inhibitors using a continuous spectrophotometric assay.

Due to the rapid enzymic activity of recombinant Mt-PrsA using the radioactive assay previously described, we sought to link Mt-PrsA catalysed AMP product release to a three-enzyme coupled assay system, thus enabling us to measure NADH oxidation at 340

nm in a continuous spectrophotometric assay, which has been described similarly elsewhere (Braven *et al.*, 1984). This system (described in Material and Methods) enabled us to record detailed measurements of the steady-state enzyme kinetics of Mt-PrsA. Plotting the steady state reaction velocity (ν) calculated from equation 1, as a function of increasing concentrations of R5P at saturating levels of ATP, results in a hyperbolic curve displaying Michelis-Menton kinetics (Fig. 5A). Nonlinear regression analysis using equation 2 derived a K_m of 8.2 μM (± 2.72 Std. Error) for R5P and a V_{max} of 530 $\mu mol^{-1}.min^{-1}.mg^{-1}$ and a specificity constant (K_{cat}/K_m) of 7.43×10^6 $M^{-1}.s^{-1}$. As previously described using the radiochemical assay, Mt-PrsA requires the presence of Pi at a concentration of 50 mM for full enzyme activation, which is illustrated in Fig. 5A. However, at reduced levels of Pi (5 mM), the subsequent addition of R5P results in partial substrate inhibition, an effect that has been observed elsewhere (Willemoes *et al.*, 2000) (data fitted to equation 3), with little or no activity recorded in the absence of Pi (Fig. 5A). This is likely due to Mt-PrsA being incompletely activated by Pi at low [Pi], meaning that at low R5P concentrations the relatively high-affinity catalytic site for R5P is occupied and normal Micheli-Menton kinetics occur until R5P reaches a concentration that results in the occupancy of a second low-affinity inhibitory site which would otherwise be occupied by Pi at higher [Pi]. Kinetic analysis of Mt-PrsA with increasing ATP concentrations at saturating levels of R5P results in a sigmoidal response showing positive cooperativity (Fig. 5b). Data obtained from measuring ν against increasing concentrations of ATP at various Pi concentrations was fitted to equation 4. At activating levels of [Pi] (50 mM), the $S_{0.5}$ and V_{max} for ATP was calculated as being 62.65 μM (± 12.04 Std. Error) and 601 $\mu mol^{-1}.min^{-1}.mg^{-1}$ (± 66.39 Std. Error) respectively. An

apparent Hill-coefficient (*n*) of 1.68 indicates strong positive cooperativity during increasing [ATP]. However, when fitted to equation 4 using nonlinear regression analysis, this effect diminishes at low [Pi] resulting in a ν vs [ATP] response with altered kinetic constants (Fig. 5b). It has been reported elsewhere that Prs enzymes from other organisms are allosterically inhibited by the presence of ADP (Arnvig *et al.*, 1990; Eriksen *et al.*, 2000; Gibson *et al.*, 1982; Switzer & Sogin, 1973; Willemoes *et al.*, 2000). We measured the effect of ADP on ν as a function of increasing [R5P] and [ATP]. At saturating concentrations of ATP, the addition of ADP resulted in non-competitive inhibition of Mt-PrsA with a calculated K_i of 320 μM (± 53.51 Std. error) against increasing [R5P] (data fitted to equation 5) (Fig. 6a). When we measured the effect of ADP on the kinetic response of Mt-PrsA to increasing [ATP] and subsequent fitting of the data to equation 6 (Fig. 6b), we calculated a K_i of 522 μM (± 45.78 Std. Error).

Biophysical characterisation of Mt-PrsA: oligomeric state and ligand binding studies

Mt-PrsA homologues from other organisms have been reported to aggregate in solution in various homo-oligomeric states, ranging from dimer to octamer (Arnvig *et al.*, 1990; Li *et al.*, 2007; Schubert *et al.*, 1975). Using analytical ultracentrifugation, we performed a set of sedimentation velocity experiments on Mt-PrsA in the absence or presence of R5P, ATP and ADP at a saturating concentrations (Fig. 7). Analysis of each experiment by interpretation of the molar mass distribution c(M), indicates that Mt-PrsA in solution alone, reaches a dynamic equilibrium between two molecular species with peaks centred over ~ 100,000 Da and ~ 205,000 Da, which relate to Mt-PrsA in a trimeric and

hexameric aggregation state respectively (Fig. 7, black line). The inclusion of 5 mM R5P showed no apparent change in the equilibrium or oligomeric state of Mt-PrsA in solution, and the c(M) vs Mw distribution aligned well with that of Mt-PrsA in the absence of ligand (Fig. 7, red line). The addition of 5 mM ATP to Mt-PrsA resulted in an altered c(M) distribution with a peak centred over ~ 70,000 Da, equating to a Mt-PrsA homodimer, and concomitant reduction in the intensity of the hexameric species, as compared to Mt-PrsA alone (Fig. 7, blue line). Interestingly, when we performed a similar experiment in combination with 5 mM ADP, the ratio of c(M) distribution shifted towards an increase in the hexameric state with a corresponding reduction in trimeric species (Fig. 7, green line). Mt-PrsA contains within its primary amino acid sequence, three naturally occurring tryptophan residues at position Trp 5, Trp 74 and Trp 188. We used Intrinsic Tryptophan Fluorescence (ITF) spectroscopy to probe the binding properties of R5P, ATP and ADP for Mt-PrsA. We performed a fluorescence emission ($F_{emission}$) scan of Mt-PrsA in solution by recording ($F_{emission}$) output between 300 and 400 nm, upon excitation at λ_{292nm}. Mt-PrsA gave a maximum fluorescence emission ($F_{emission}^{max}$) at a wavelength of 335 nm, thus providing a basal $F_{emission}$ coordinate for the collection of subsequent ITF data. The change in fluorescence emission ($\Delta F_{emission}$) was calculated by subtracting the $F_{emission}$ (recorded 5 min after each ligand titration) away from ($F_{emission}^{max}$), and the data was then plotted against [L]. Nonlinear regression analysis of $\Delta F_{emission}$ vs [R5P] using equation 7 shows a hyperbolic isothermal ligand binding curve for R5P, with a calculated K_d of 24.8 μM (± 6.77 Std. Error) (Fig. 8a). We sought to investigate what effect ATP might have on the K_d for R5P, however, the inclusion of both ATP and R5P would obviously result in enzyme catalysis and the

formation of pRpp and AMP. Due to the relatively high specific activity of Mt-PrsA, the addition of R5P and ATP at concentrations required for the effective measurement of ligand binding constants by ITF would result in a reaction that would go to completion within the 5 min time-frame required to establish binding equilibrium. Therefore, due to the stability of the imido-diphophate moity and lack of enzyme-catalysed phosphate transfer, we used the ATP analogue 5'-adenylyl-β,γ-imidodiphosphate (AMPPNP) as an ATP ligand substitute for binding assays, when carried out in conjunction with R5P. Mt-PrsA was titrated with increasing [AMPPNP] using identical increments carried out during ATP ligand binding experiments. Subsequent nonlinear regression analysis and comparison of the $\Delta F_{emission}$ vs [AMPPNP] and $\Delta F_{emission}$ vs [ATP] plots (data not shown) resulted in a strong correlation (R^2 = 0.986) as well as extremely similar dissociation constants of 28.29 μM (± 0.54 Std. Error) and 31.02 μM (± 0.62 Std. Error) for ATP and AMPPNP respectively. With similarly calculated Hill-coefficients (n) of ~4, the almost identical binding properties of ATP and AMPPNP for Mt-PrsA allowed us to confidently substitute AMPPNP for ATP during binding assays carried out in combination with R5P. In this regard, when R5P was titrated against Mt-PrsA in the presence of 5 mM AMPPNP, the apparent K_d for R5P decreased to 21.36 μM (± 4.84 Std. Error). This data indicates that the Mt-PrsA-AMPPNP complex exhibits a slightly higher affinity for R5P when compared to Apo-Mt-PrsA (Fig. 8a). In the reverse experiment where $\Delta F_{emission}$ vs [AMPPNP] was measured in the presence or absence of 5 mM R5P (Fig. 8b), the affinity of Mt-PrsA-R5P for AMPPNP increased slightly, as is evident from the reduction in K_d to 28.22 μM (± 0.54 Std. Error) and an increase in the Hill-coefficient (n) to 5 by a value of 1. In light of the previous AUC experiment, which suggests that the addition of ADP

induces a shift towards Mt-PrsA hexamerisation, we performed an ITF experiment by tritrating Mt-PrsA with increasing [ADP] (Fig. 9a). Unsurprisingly, the $\Delta F_{emission}$ vs [ADP] plot displays a sigmoidal cooperative binding response with an apparent K_d of 512.6 μM (± 39.57 Std. Error) and a Hill-coefficient of 2. Since ATP and ADP bind to Mt-PrsA at separate sites, and induce very different aggregation states, the apparent ~2 fold difference in the F_{max} recorded for ATP and ADP is most likely due to the differing effects each of these ligands have on the chemical environments surrounding the tryptophan residues providing the source of $F_{emission}$ in Mt-PrsA (Eriksen *et al.*, 2000). The inclusion of ADP at two different concentrations (0.1 and 2.0 mM) in separate ITF [ATP] ligand binding assays, causes a significant increase in the apparent K_d of ATP for its Mt-PrsA binding site (K_d^{ATP} = 31.22 μM and 90.1 μM at a concentration of 0.1 and 2.0 mM ADP respectively), clearly illustrating allosteric inhbition of Mt-PrsA-ATP complex formation (Fig. 9b). The change in the slope of the curve as a function of [ATP] in separate ITF experiments carried out at increasing ADP concentrations, clearly illustrates a reduction in the homotropic cooperative binding of ATP for Mt-PrsA, which was confirmed by calculating the resultant Hill-coefficients (Fig. 9b). The ligand binding properties of ADP for Mt-PrsA, in the presence of ATP, compares well with the inhibition constant calculated for ADP [K_i = 522 μM (± 45.78 Std. Error)] obtained from kinetic analysis of ν vs [ATP] at saturating [R5P] (Fig. 6b).

Structural model of Mt-PrsA

An alignment of Mt-PrsA with its related *Corynebacterineae* PrsA orthologues as well as othet bacterial Prs homologues from *Bacillus subtilis* (Bs_PrsA), *Escherichia coli*

(Ec_PrsA) and *Streptomyces coleicolor* (Sc_PrsA), and the three human Prs isoforms (Human_PrsA1-3) clearly illustrates the high level of primary sequence conservation between all variants (Fig. 10). Mt-PrsA shares very high sequence identity with its *Corynebacterineae* counterparts (92 % *Mycobacterium leprae*, 87 % *Mycobacterium smegmatis* and 71 % *Corynebacterium glutamicum*) and a moderate level of sequence identity with Mt-PrsA homologues in *S. coleicolor* (61 %), *E. coli* (43 %) and *B. subtilis* (43 %). Interestingly, the three human Prs isoforms also share 40 % sequence identity with Mt-PrsA. Both of the human type 1 and B. subtilis pRpp synthetase X-ray crystal structures have been solved (Eriksen *et al.*, 2000, Sheng *et al.*, 2007). Each of these structures were solved in the Apo form and in complex with AMP, which is located in the ATP binding pocket of the active site. Interestingly, the Bs-PrsA structure was solved in complex with an additional molecule of ADP, thus revealing its position and mode of action in the allosteric regulatory site of the enzyme (Eriksen *et al.*, 2000). Since Mt-PrsA shares highest sequence homology with Bs-PrsA, we constructed a homology model of Mt-PrsA using the structure of Bs-Prs in complex with AMP and ADP as a template (Eriksen *et al.*, 2000) (Fig. 11). Using crystallographic symmetry data from the Bs-Prs structure, we arranged the Mt-PrsA homology model into its hexameric form (Fig. 11a). Each monomer is composed of two subunits, which is related by a 3-fold axis perpendicular to an additional 2-fold planar rotational symmetry. Many of the residues involved in binding at the interface between monomers are well conserved, with notable differences highlighted by the position of red spheres in Fig. 11a. With only a few exceptions, the sequence alignment of Mt-PrsA and Bs-Prs indicates that most of the residues involved in enzyme catalysis and allosteric regulation are conserved which, in

turn, are suitably positioned in the Mt-PrsA homology model compared to Bs-Prs. A noteworthy difference in the Mt-PrsA catalytic site is the presence of Asn45, which is arranged to form contacts with the ADP ligand (Fig. 11b). In the Bs-Prs structure, the equivalent residue is Asp42. In addition, further comparison of the two structures suggests that the Mt-PrsA homology model retains all of the important residues required for the regulatory site, apart from Gly88 (Ala85 in Bs-Prs), which participates in the formation of contacts to ADP with a neighbouring Ser89 (Fig. 11b). An interesting observation in the model of Mt-PrsA is the presence of His109 in the "flexible loop" formed by Mt-PrsA residues Lys108 – Arg112. Ala106 is the equivalent residue in Bs-Prs, and it appears to play little if no part in binding or coordination of the ADP ligand. This flexible loop region, which contains many conserved residues (Fig. 10), has been identified as displaying some of the largest variation in backbone conformation, and the conformational changes that occur upon substrate binding are considered to be important for catalysis (Eriksen *et al.*, 2000). The presence of a His residue in the Mt-PrsA flexible loop region might allow for multiple hydrogen bonding opportunities between His109 and the ATP substrate in the catalytic site (Fig. 11b). Gly111 is another conserved residue located in the flexible loop of mycobacterial PrsA enzymes, which in the majority of other bacterial homologues, is typically replaced by a Ser that makes H-bond interactions with the α-phosphate of ADP in the allosteric site (Fig. 11c). Both the Human-PrsA1 and Bs-PrsA homodimers are stabilised by a salt bridge at the N-terminal interface formed between two conserved residues (Asn114 and Asp139, and Asn120 and Asp145 respectively) (Eriksen *et al.*, 2000, Sheng *et al.*, 2007). From the sequence alignment and Mt-PrsA homology model, it is worth noting that the equivalent Asn residue is replaced

by an aspartic acid (Asp122) which would sit in close proximity to Asp147. Therefore, it is reasonable to assume that unlike Human-PrsA1 and Bs-PrsA, a salt bridge does not occur at the Mt-PrsA dimer interface. Interestingly, the Human-PrsA1 Asn114 (Asp122 in Mt-PrsA) is often mutated to a Ser in the cells of patients suffering from gout (Becker, *et al*., 1995). It has been reported that the molecular mechanism behind the 50% increase in N114S mutant enzyme activity is caused by a disruption of a salt bridge, which would otherwise stabilises the dimer interface (Liu *et al*., 2009).

Discussion

The presence of D-arabinose in living organisms is rarely observed. Whilst the utilisation of D-arabinopyranose seems to be confined to glycoconjugate formation in trypanosomatid parasites (Turnock & Ferguson, 2007), arabinose in the furanose configuration (Ara*f*) is exclusively used by bacteria in the formation of cell surface polysaccharides and the biosynthesis of glycolipid antigens. Members belonging to the *Corynebacterineae*, such as *M. tuberculosis* and *C. glutamicum*, contain large quantities of Ara*f* in the form of arabinan, which in turn, is covalently attached to galactan and mannan, thus forming AG and LAM respectively. Whilst LAM exerts its biological activity by subverting the host immune response, the primary function of AG is to provide a highly branched molecular scaffold, linking the murine sacculus to the hydrophobic mycolate layer. Since arabinan is an essential component of the TB cell wall and is targeted by treatment with EMB, other enzymes involved in its formation might present themselves as potential putative drug-targets. In this regard, DPPR synthetase (Rv3806c) is a novel enzyme catalysing the transfer of pRpp to decaprenol-1-

monphosphate forming DPPR (Fig. 1) and represents the first committed step towards the biosynthesis of DPA (an exclusive cell wall AraT substrate) and as a consequence of its genetic disruption in *C. glutamicum* (a model organism used to study *M. tuberculosis* cell wall physiology), affords a phenotype displaying retarded growth, and a severely altered cell wall composition which is completely deficient in arabinan (Alderwick *et al*., 2005). In addition, DprE1 (Rv3790) has been shown to be the molecular target of benzothiazinones, a new class of antimycobacterial agents, which can effectively kill MDR and XDR strains of TB by blocking the C2-OH epimerisation of DPR to DPA (Makarov *et al.*, 2009). Some of the current front line drugs used to treat TB include cell wall inhibitors. However, the incidence of MDR and XDR-TB cases is alarmingly high and continues to rise (Madariaga *et al.*, 2008). Since the *M. tuberculosis* cell wall is a valid drug target, we must continue to investigate the physiology, biochemistry and metabolic pathways involved in its assembly, to assist our efforts of developing new anti-TB therapies. However, non-dividing drug-tolerant populations of "persistent" TB bacilli fail to be eradicated from the host, giving rise to a latent infection as result of subsequent granuloma formation (Barry *et al.*, 2009). Inhibition of cell wall biosynthetic processes of TB bacilli responsible for latent infections is of no consequence, this being due to the fact that persistent TB bacilli are not undergoing active cell growth and division. However, these "dormant" TB-bacilli still require a basal level of "energy" metabolites in order to maintain critical cellular functions (Koul *et al.*, 2008).

pRpp is a central metabolite ubuiquitous in nature providing a high-energy substrate for the biosynthesis of histidine, tryphophan, NAD, NADP and both the *de novo* and salvage

pathways involved in nucleoside metabolism (Hove-Jensen, 1988) (Fig. 1). In addition to these central metabolic processes, the *Corynebacterineae* have evolved a unique pathway in which pRpp is siphoned into cell wall arabinan biosynthesis (Fig. 1). In *M. tuberculosis*, Mt-PrsA is entirely responsible for the provision of pRpp and its cellular function bridges five different metabolic pathways (Fig. 1). The omphalic nature of Mt-PrsA places a heavy burden on its biological function, especially during cell growth and division, when the cellular requirement for pRpp increases significantly. In this study, we describe the biochemical characterisation of Mt-PrsA, which displays the highest recorded specific activity for a pRpp synthetase of 530 $\mu mol^{-1}.min^{-1}.mg^{-1}$. The K_m for R5P was calculated to be in the sub-micromolar range of (8.2 μM), suggesting a rapid enzyme turnover with a calculated specificity constant (K_{cat}/K_m) of 7.4×10^6 $M^{-1}.s^{-1}$. This relatively high efficiency of Mt-PrsA fits well with the physiological function of the enzyme during cell wall biosynthesis, considering the increased demand for pRpp that is required for antecedent DPA biosynthesis. Mt-PrsA displays clear homotropic cooperativity for ATP, with an apparent $S^{0.5}$ 62.65 μM, which is extremely low considering the intracellular concentration of ATP is considered to be between 3 – 5 mM. The homology model generated for Mt-PrsA contains many structural features of other pRpp synthetases that have been solved to date. The majority of the active site residues modelled in Mt-PrsA are conserved with those from other Mt-PrsA homologues, and it appears that the appropriate configuration of amino acid side chains compares well with the *B. subtilus* structure. This is also the case for the regulatory site in which ADP binds to allosterically modulate the enzyme. However, an interesting observation is the presence of His109 in the flexible loop region of Mt-PrsA, a residue exclusively

conserved within members of the *Corynebacterineae*. Considering the close proximity of His109 to both the catalytic and regulatory sites of Mt-PrsA, and its potential to make direct contacts with both ATP and ADP ligands, the presence of this conserved His in the flexible region of mycobacterial pRpp synthetases might provide some explanation for the relatively high K_{cat}. pRpp synthetase superactivity is observed in human type-1 N114S mutants (Becker, *et al*., 1995). This is increase in activity is a result of the loss of a salt bridge formed between two monomers which induces small but significant changes to the catalytic and regulatory site of the enzyme (Liu *et al*., 2009). Interestingly, the homology model of Mt-PrsA suggests that a slat bridge between the equivalent residues does not occur thus reducing the stability of the dimer interface. In mycobacteria, the biosynthesis of pRpp is required at a rate which is sufficient to not only supply central metabolic processes, such as *de novo* nucleoside biosynthesis, but also at a necessary level to meet the increased demands for pRpp during cell wall biosynthesis (Scherman *et al.*, 1995; Scherman *et al.*, 1996). It seems plausible that pRpp synthetases from *Corynebacterineae* species have evolved a highly efficient version of the enzyme to account for the increased metabolic flux of pRpp, during various physiological states. pRpp synthetases in other organisms undergo stringent control by virtue of allosteric modulation from ADP. In this regard, Mt-PrsA also appears to be no different, displaying clear inhibition of enzyme activity between 0.5 - 2.0 mM ADP. When taken together, the data relating to ADP inhibition and the subsequent complex formation with Mt-PrsA, suggests that the mechanism employed for allosteric regulation of Mt-PrsA by ADP, is through the formation of a Mt-PrsA hexamer (Arnvig *et al.*, 1990). This net increase in Mt-PrsA hexamer oligimerisation suggests that the efficacy of ATP for its Mt-PrsA

catalytic site decreases, as a consequence of ADP allosteric modulation. The three human PrsA isoforms share a very high sequence identity (91 - 95 % between all three), however the subtle differences that do occur appear in regions of the enzyme which are important for catalysis and allosteric regulation. Inhibition studies using two aminopyrimidopyrimidine nucleotide analogues 4-methoxy-8-(β-D-ribofuranosylamino)-pyrimido-[5,4-d]-pyrimidine (MRPP) and 4-amino-8-(β-D-ribofuranosylamino)-pyrimido-[5,4-d]-pyrimidine (ARPP) show differential levels of inhibition of human pRpp synthetases (Fry *et al.,* 1995). Carbocyclic analogues of ribose-5-phosphate are another class of compounds which show differential inhibition when tested against *Salmonella typhimurium*, *B. subtilis* and human pRpp synthetases (Parry *et al*., 1996). In this regard, the development of a similar library of compounds targeted for the specific inhibition of Mt-PrsA might warrant further investigation. Understanding metabolic pathways that are essential for persistent TB infections, such as mycobacterial energy metabolism, in combination with pathways involved in cell wall assembly seems a plausible strategy for the development of new anti-mycobacterial drugs.

Materials and Methods

Bacterial strains cloning procedures

Escherichia coli Top 10 cells (Invitrogen) were used to propagate plasmids during all cloning experiments and the over-expression of Mt-PrsA was carried out in *E. coli* C41 (DE3) (Lucigen). Phusion DNA polymerase was purchased from New England Biolabs and all restriction enzymes and T4 DNA ligase were purchased from fermentas. Oligonucleotides were purchased from eurofins-MWG and PCR fragments were purified

using QIAquick gel extraction kit (Qiagen). Plasmids were purified using the Qiaprep purification kit (Qiagen).

Generation of *C. glutamicum prsA*-null mutant

For the genomic disruption of *NCgl0945* (*Cg-prsA*), we constructed the plasmid pK18mob-*Cg-prsA*-int, using the primer pair pNCgl0945_intfor (GCGAGCCAATTTCTGCTCGC) and pNCgl0945_intrev (GACAACCTGGTTTGCTACCTC) to amplify *C. glutamicum* WT chromosomal DNA. The resulting DNA fragment was treated with AvaI/KpnI, and ligated into the non-replicative vector pK18mob (Schafer *et al.*, 1994), which was similarly treated with AvaI/KpnI. The DNA integrity of the resulting construct pK18mob-*Cg-prsA*-int was confirmed by sequencing and used for transformation of *C. glutamicum* by electroporation and selected for resistance to kanamycin at 25 μg/ml on BHIS medium.

Construction of Mt-PrsA expression vector

The 981-bp coding region for Mt-PrsA (annotated as Rv1017c) in the *M. tuberculosis* H37Rv genome was amplified by PCR using the following primer pairs (restriction sites underlined) GATCGATCGCTAGCTTGAGCCACGACTGGACCGATAATCGC (forward) and GATCGATCCTCGAGTGCGTCCCCGTCGAAAAGTCCTGTTAC (reverse). This DNA fragment was restricted with the appropriate enzymes (NheI and XhoI) and ligated into pET23b digested with identical enzymes, thus yielding pET23b-

Mt-prsA, which encodes for an C-terminal His_6-tagged protein. DNA sequencing and construct verification was carried out at the University of Birmingham School of Bioscience Genomics Facility.

Expression and Purification of Mt-PrsA

E. coli C41 (DE3) cells were transformed with pET23b-*Mt-prsA* and selected on LB agar supplemented with 100 μg/mL amplicillin. Recombinant *E. coli* cells harbouring pET23b-*Mt-prsA* were used to inoculate an overnight of 5mL LB supplemented with 100 μg/mL amplicillin. This overnight was then used to inoculate 2 x 1 L LB medium supplemented with 100 μg/mL amplicillin and incubated at 37 °C with shaking until A_{600} reached 0.5. IPTG was then added at a final concentration of 1 mM and growth continued for an additional 12 h at 16 °C with shaking. Cells were harvested by centrifugation at 6000*g* for 15 mins and washed with 20 mL phosphate buffered saline. Pellets were then frozen until further use. For purification, one pellet was thawed and re-suspended into 50 mM KH_2PO_4 (pH 7.9), 300 mM NaCl, 20 mM imidazole, one complete protease inhibitor cocktail tablet (Roche) and DNAse and RNAse both at a final concentration of 50 μg/mL. The cell suspension was disrupted by sonication at a pulse rate of 30 sec ON and 30 sec OFF for a total of 10 cycles. The cell slurry was centrifuged for 30 min, 28000*g* at a temperature of 4 °C. The supernatant was collected and passed over a 5 mL HiTrap Ni^{2+}-NTA agarose column (GE Healthcare), which was previously equilibrated with into 50 mM KH_2PO_4 (pH 7.9), 300 mM NaCl and 20 mM imidazole. Elution occurred *via* a stepwise gradient of 50 – 500 mM imidazole in 50 mM KH_2PO_4 (pH 7.9), 300 mM NaCl and 10 mL fractions were collected. Mt-PrsA was detected to be present and ~ 98 % pure

in the 250 mM imidazole fraction, as determined by 12% SDS-PAGE analysis. The 250 mM imidazole fractions of Mt-PrsA was first dialysed against 2 L KH_2PO_4 (pH 7.9), 150 mM NaCl, 5 mM EDTA and 1 mM DTT at 4 °C and then against 2 L KH_2PO_4 (pH 7.9), 150 mM NaCl, 1 mM DTT and 10 % glycerol. After dialysis, the protein concentration was determined using the bicinchoninic acid procedure (Pierce) and bovine serum albumin as a standard.

Preparation of [^{14}C]-U-D-ribose-5-phosphate

We prepared a source of [^{14}C]-U-D-ribose-5-phosphate ([^{14}C]-R5P) using a modified process as described in (Boss *et al.*, 1984),for the subsequent use in Mt-PrsA assays. 100 μCi of [^{14}C]-U-D-glucose (100 μl in 70 % ethanol) (ARC radiochemicals) was dried in 14 ml glass tube under compressed nitrogen and then resuspended in 500 μl of 50 mM KH_2PO_4 (pH 7.9), 150 mM NaCl, 5 mM $MgCl_2$ and 0.5 mM $MnCl_2$. 20 μl of ATP (100 mM stock) and 20 μl of NADP (100 mM stock) was added to the suspension. 20 μl of hexokinase/glucose-6-phosphate dehydrogenase enzyme mix (Roche) was added and incubated at 37 °C for 15 mins. A few grains of 6-phosphogluconic dehydrogenase (Sigma) and a further 20 μl of NADP (100 mM stock) was added and incubated for 15 mins at 37 °C. A few grains of phosphoribose mutase (Sigma) was added to the reaction mix and incubated for a further 15 mins at 37 °C followed by another addition of 20 μl NADP (100 mM stock) and final incubation at 37 °C for 15 mins. The reaction mix was then diluted with H_2O to a final volume of 3 mL and passed through a 10 kDa MWCO centrifugal filtration device (Millipore). The filtrate (~ 3 mL) was then loaded onto a 3 mL LC-SAX anion exchange cartridge (Supelco) pre-equilibrated with H_2O. The column

was then washed three times with 3 mL H_2O. The column was then washed with a 100-1000 mM stepwise gradient of sodium acetate (3 mL fractions of 100 mM increments). Each fraction (1 μl) was applied to a glass-backed PEI-cellulose TLC plate and developed in 0.85 M KH_2PO_4 (pH 3.4). After drying, the TLC plate was exposed overnight to a Kodak autoradiography film for visualisation of radioactive phospho-sugars. [^{14}C]-R5P eluted as a single band (as compared to known standards) in the 200 mM sodium acetate fraction with a specific activity of 33333 cpm/μl.

Radiochemical assay of Mt-PrsA activity

The enzymatic activity of Mt-PrsA was determined by monitoring the transfer of PPi from ATP to the C1-OH group of enzymaticaaly synthesised [^{14}C]-R5P forming p[^{14}C]Rpp and AMP. The basic reaction mix contained 50 mM KH_2PO_4 (pH 7.5), 150 mM NaCl, 1mM DTT, 10 % glycerol, varying amounts of [^{14}C]-D-R5P [stored in 200 mM sodium acetate, (33333 cpm/μl)], 2 mM ATP and 30 μg Mt-PrsA (15 μl) in a final volume of 100 μl. On occasions, $MgCl_2$, $MnCl_2$, $CaCl_2$, ADP and EDTA were included in the reaction mix either separately or combination, all at a final concentration of 2 mM. Reactions were initiated by the addition of Mt-PrsA and incubated at 37 °C for 10 mins. Reactions were quenched by the addition of 10 μl 0.4 M formic acid. The mixture (1.1 μl) was applied to a glass-backed PEI-cellulose TLC plate and developed in 0.85 M KH_2PO_4 (pH 3.4). After drying, the plate was inspected for radioactive spots by either exposure to a Kodak film followed by autoradiography or a PhosphorImager (Molecular Dynamics). All experiments were repeated in triplicate.

Metabolism of [^{14}C]-R5P into mycobacterial cell wall biosynthetic precursors

Membranes (containing membrane bound enzymes involved in lipid-linked cell wall biosynthetic processes) and "P60" (a percoll-derrived cell free fraction rich carbohydrate and enzymes associated with cell wall processes as described in (Besra *et al.*, 1997)) fractions from *M. smegmatis* were prepared as described previously (Alderwick *et al.*, 2006a; Besra *et al.*, 1997; Lee *et al.*, 1997) and resuspended in buffer A [50 mM MOPS (pH 7.9), containing 5 mM β-mercaptoethanol and 10 mM $MgCl_2$] to a final concentration of 15 mg/ml and 10 mg/ml for membrane and P60 fractions, respectively. 50 μg of decaprenol-1-monophosphate (Larodan Lipids, Malmo, Sweeden) (5 mg/ml stored in $CHCl_3$/CH_3OH (2:1, v/v)) was dried in a 1.5 ml eppendorf tube under compressed nitrogen and was resuspended by the addition of 10 μl of a solution of 50 mM MOPS (pH 7.9), 50 mM KH_2PO_4, 150 mM NaCl, 1 mM $MnCl_2$, 1 mM $MgCl_2$, 1 mM DTT and 1% IgePal CA-630 (Sigma) followed by bath sonication. The basic assay mix consisted of 0.5 mg *M. smegmatis* membranes (33 μl), 2 mM ATP, 50 mM MOPS (pH 7.9), 50 mM KH_2PO_4, 150 mM NaCl, 1 mM $MnCl_2$, 1 mM $MgCl_2$, 1 mM DTT, 100,000 cpm [^{14}C]-R5P (3 μl) in a final volume of 200 μl. $NaWO_4$ and NaF as well as ADP were included in separate assay reactions at a final concentration of 2 mM for all inhibition studies. 0.5 mg of *M. smegmatis* P60 (50 μl) was added a where appropriate. Reactions were initiated by the addition of 30 μg of Mt-PrsA (15 μl) and incubated at 37 °C for 30 mins. Assays were quenched by the addition of 1.33 ml of $CHCl_3$/CH_3OH (1:1, v/v), mixed for 30 mins and centrifuged at 27,000*g* to remove precipitated proteiacous material. The supernatent was removed to a separate tube and combined with 670 μl $CHCl_3$ and 287 μl H_2O, mixed for 15 mins and centrifuged for 5 mins at 4000*g* to form a

biphase. The lower organic phase was removed and washed twice with 765 µl $CHCl_3/CH_3OH/H_2O$ (3:47:48, v/v/v) and then dried under compressed nitrogen. Samples were the resuspended in 100 µl $CHCl_3/CH_3OH$ (2:1, v/v) and an aliquot subject to TLC analysis using silica gel plates (5735 silica gel 60F254, Merck) developed in $CHCl_3/CH_3OH/CH_3COONH_4/NH_4OH/H_2O$ (180:140:9:9:23 v/v/v/v/v) and visualised by autoradiography by exposure of TLCs to X-ray film (Kodak X-Omat) as described in (Mikusova *et al.*, 2005).

Metabolism of [^{14}C]-R5P into mycobacterial cell wall biosynthetic precursors and the subsequent AraT-dependent transfer to a neo-glycolipid acceptor.

Membranes and P60 from *M. smegmatis* were prepared as described above. The neo-glycolipid acceptor used in this study was the disaccharide α-D-Ara*f*-(1→5)-α-D-Ara*f*-*O*-$(CH_2)_7CH_3$ (Ara_2) which has been previously reported by us (Lee *et al.*, 1997; Seidel *et al.*, 2007). In individual assays, the Ara_2 acceptor 8 µl (stored in $CHCl_3/CH_3OH$, 2:1, v/v at 20 mM) and 50 µg of decaprenol-1-monophosphate (Larodan Lipids, Malmo, Sweeden) (5 mg/ml stored in $CHCl_3/CH_3OH$ (2:1, v/v)) was aliquoted into 1.5 ml eppendorf tubes and dried under nitrogen. The AraT assay was carried out as described previously (Lee *et al.*, 1997; Seidel *et al.*, 2007) with modifications. IgePal^{TM} (Sigma-Aldrich) was added (0.1%, v/v) with the appropriate amount of buffer A (final volume 100 µl). Tubes were sonicated for 15 min to resuspend lipid linked substrates and then mixed with the remaining assay components, which included 0.5 mg *M. smegmatis* membranes (33 µl), 0.5 mg *M. smegmatis* P60 (50 µl), 30 µg Mt-PrsA (15 µl), 1 mM ATP, 1 mM NADP and in some cases EMB (100 µg/ml). Assays were incubated for 1 h

at 37°C and quenched by the addition of 633 µl $CHCl_3/CH_3OH$ (1:1, v/v). After mixing and centrifugation at 27000*g* for 15 min at 4°C, the supernatant was removed and dried under nitrogen. The residue was then resuspended in 700 µl of CH_3CH_2OH/H_2O (1:1, v/v) and loaded onto a 1 ml LC-SAX strong anion exchange cartridge (Supelco), pre-equilibrated with CH_3CH_2OH/H_2O (1:1, v/v). The column was washed with 2 ml CH_3CH_2OH and the eluate collected, dried and partitioned between the two phases arising from a mixture of *n*-butanol (3 ml) and water (3 ml). The resulting organic phase was recovered following centrifugation at 3,500*g* and the aqueous phase again extracted twice with 3 ml of water-saturated *n*-butanol. The pooled extracts were back-washed twice with *n*-butanol-saturated water (3 ml). The *n*-butanol fraction was dried and resuspended in 200 µl butanol. The extracted radiolabeled material was quantified by liquid scintillation counting using 10 % of the labelled material and 5 ml of EcoScintA (National Diagnostics, Atlanta). The incorporation of [^{14}C]-Ara*f* into Ara_2 was determined by subtracting counts present in control assays (incubations in the absence of acceptor). The remaining labelled material was subjected to TLC using $CHCl_3$:CH_2OH:H_2O:NH_4OH (65:25:3.6:0.5, v/v/v/v) on aluminium-backed silica gel plates (5735 silica gel 60F254, Merck) and products were visualised by autoradiography, exposing the TLCs to X-ray film (Kodak X-Omat).

Continuous enzyme-coupled spectrophotometric assay and kinetic characterisation of Mt-PrsA substrates.

By using a modified assay described by Braven *et al.*, (1984), the amount of AMP produced as a product of Mt-PrsA catalysis was measured indirectly by monitoring the

decrease in absorbance of NADH at 340 nm *via* the following enzyme couple: **1.** R5P + ATP → pRpp + AMP, catalysed by Mt-PrsA; **2**. AMP + ATP → 2 ADP, catalysed by myokinase (MK); **3.** 2 ADP + 2 phosphoenolpyruvate (PEP) → 2 pyruvate + 2 ATP, catalysed by pyruvate kinase (PK) and **4.** 2 pyruvate + 2 NADH + 2 H^+ → 2 lactate + 2 NAD^+, catalysed by lactate dehydrogenase (LDH). This perpetual enzyme couple immediately replenishes the pool of ATP and results in a stoichiometry of 1 mole of NADH oxidised by lactate dehydrogenase for every 2 moles of AMP produced by Mt-PrsA. The following formula was used to calculate the rate of reaction thus allowing for a detailed kinetic characterisation of Mt-PrsA,

$$v = (\Delta A.s^{-1})/2 \times 6220\ M^{-1} \qquad \text{(Equation 1)}$$

where ν is the steady-state rate of the reaction, Δ*A* is the change in absorbance at 340 nm and 6220 M^{-1} is the molecular extinction coefficient of NADH measured at 340 nm. The reaction mixture comprised of 50 mM KH_2PO_4 (pH 7.9), 150 mM NaCl, 0.25 mM DTT, 2 mM $MnCl_2$, 2.0 mM PEP, 1.0 mM NADH, and 5 mM NaF, MK, PK and LDH were added to the mix all at a concentration of 0.2 units/mL. Variable amounts of ATP, R5P and ADP were added to the reaction mix for enzyme kinetic and inhibitor studies. Reactions were initiated by the addition of R5P. All kinetic experiments were carried out in triplicate (from three different independent protein preparations of purified recombinant Mt-PrsA) and data points (calculated mean) and standard errors (± Std. Error) relating to enzyme steady state velocities (ν) (μmol.min^{-1}.mg^{-1}) derived from equation 1 under various substrate and inhibitor conditions, was analysed by nonlinear

regression analysis and fitted to the appropriate equation (2-6) using the GraphPad Prism software package. Equation 2 is the Michelis-Menten equation for hyperbolic substrate saturation kinetics and equation 3 applies to nonlinear regression of substrate inhibition. Equation 4 is the Hill equation for calculating cooperative substrate saturation kinetics, equation 5 applies to noncompetitive enzyme inhibition of a hyperbolic enzyme response and equation 6 is derived from combining equations 4 and 5 to give an expression for noncompetitive enzyme inhibition of a cooperative sigmoidal response to increasing substrate concentrations.

$$\nu = V_{max} \times S / (K_m + S) \qquad \text{(Equation 2)}$$

$$\nu = V_{app} \times S / [K_m + S \times (1 + S/K_i)] \qquad \text{(Equation 3)}$$

$$\nu = V_{app} \times S^n / (S_{0.5}{}^n + S^n) \qquad \text{(Equation 4)}$$

$$\nu = V_{app} \times S / [K_m(1 + I/K_{is}) + S(I + I/K_{ii})] \qquad \text{(Equation 5)}$$

$$\nu = V_{app} \times S^n / [S_{0.5}{}^n (1 + I/K_{is}) + S^n(1 + I/K_{ii})] \qquad \text{(Equation 6)}$$

where V_{max} is the maximum enzyme velocity, V_{app} is the apparent maximal enzyme velocity, S is the concentration of the substrate being varied, I is the inhibitor concentration, K_m is the apparent Michelis-Menten constant for S, $S_{0.5}$ is the half-saturation concentration for S, n is the apparent Hill-coefficient for S, K_{is} and K_{ii} are the dissociation constants of the [I], for E and ES respectively.

Analytical ultracentrifugation

Sedimentation velocity experiments were performed using a Beckman Optima XL-A analytical ultracentrifuge equipped with absorbance optics. Mt-PrsA (dialysed into 50 mM KH_2PO_4 (pH 7.9), 300 mM NaCl, 1 mM DTT) was loaded into cells with two channel Epon centre pieces and quartz windows. A total of 100 absorbance scans (280 nm) were recorded (40,000 rpm, 4°C) for each sample, representing the full extent of sedimentation of the sample. Data analysis was performed using the SEDFIT software fitting a single friction coefficient (Schuck, 2004).

Intrinsic Tryptophan Fluorescence spectroscopy

Intrinsic tryptophan fluorescence experiments were carried out using a PTI QuantaMaster^{TM} 40 spectrofluorimeter and data recorded using FeliX32 software. The excitation wavelength was set at 292 nm and the fluorescence emission ($F_{emmison}$) spectra was recorded between 300 – 400 nm for each ligand aliquot added to a 200 µl solution containing 70 µM Mt-PrsA 50 mM KH_2PO_4 (pH 7.9), 150 mM NaCl, 0.25 mM DTT, 2 mM $MnCl_2$ was used as a buffer for the measurement of R5P, ATP and AMPPNP ligand binding (or a combination) to Mt-PrsA. A plot of the change in fluorescence emission ($\Delta F_{emisson}$) intensity at λ_{335nm} vs. [L] was fitted to equation 7 for R5P, equation 8 for ATP and ADP for independent additions, equation 9 for R5P in combination with AMPPNP and equation 10 for ATP and ADP in combination using GraphPad Prism software.

$$\Delta F_{emission} = F_{max} \times L / (K_d + L) \qquad \text{(Equation 7)}$$

$$\Delta F_{emission} = F_{max} \times L^n / (K_d^n + L^n) \qquad \text{(Equation 8)}$$

$$\Delta F_{emission} = F_{max}{}^{a} \times L^{a} / (K_d + L^{a}) + F_{max}{}^{b} \times L^{nb} / (K_d{}^{nb} + L^{nb}) \quad \text{(Equation 9)}$$

$$\Delta F_{emission} = F_{max}{}^{a} \times L^{na} / (K_d{}^{na} + L^{na}) + F_{max}{}^{b} \times L^{nb} / (K_d{}^{nb} + L^{nb}) \quad \text{(Equation 10)}$$

where F_{max} indicates the maximum change in fluorescence emission, K_d is the concentration of ligand required to achieve half maximum fluorescence, L is the concentration of ligand and n is the Hill-coefficient. The suffixes a and b relate to the relative parameters determined for two separate ligands included in a binding assay.

Generation of a Mt-PrsA homology model

A homology model of the molecular structure of Mt-PrsA was derived based on the crystal structure of *B. subtilus* Prs (Eriksen *et al.*, 2000). Models were obtained from several Web-based moedelling servers, including SWISS-MODEL (Schwede *et al.*, 2003), Geno3D (Combet *et al.*, 2002) and 3D-JIGSAW (Bates *et al.*, 2001). The homology models were analysed in comparison to the the Bs-Prs structures in complex with SO_4^- or mADP (PDB entry 1DKR and 1DKU (Eriksen *et al.*, 2000)).

Acknowledgements

G.S.B. acknowledges support in the form of a Personal Research Chair from Mr. James Bardrick, Royal Society Wolfson Research Merit Award, as a former Lister Institute-Jenner Research Fellow, the Medical Research Council, and The Wellcome Trust (081569/Z/06/Z).

Abbreviations

Arabinogalactan (AG), decaprenol-1-monophosphate (DP), decaprenol-1-monophosphorarabinose (DPA), decaprenol-1-monophosphoribose (DPR), decaprenol-1-monophosphoribose-5-phosphate (DPPR), decaprenol-1-monophosphoryl-2-keto-β-*erythro*-pentofuranose (DPX), phosphoribosylpyrophosphate (pRpp), lipoarabinomannan (LAM), ribose-5-phosphate (R5P).

References

Alderwick, L. J., Radmacher, E., Seidel, M. & other authors (2005). Deletion of *Cg-emb* in *Corynebacterianeae* leads to a novel truncated cell wall arabinogalactan, whereas inactivation of *Cg-ubiA* results in an arabinan-deficient mutant with a cell wall galactan core. *The Journal of biological chemistry* 280, 32362-32371.

Alderwick, L. J., Dover, L. G., Seidel, M., Gande, R., Sahm, H., Eggeling, L. & Besra, G. S. (2006a). Arabinan-deficient mutants of *Corynebacterium glutamicum* and the consequent flux in decaprenylmonophosphoryl-D-arabinose metabolism. *Glycobiology* 16, 1073-1081.

Alderwick, L. J., Seidel, M., Sahm, H., Besra, G. S. & Eggeling, L. (2006b). Identification of a Novel Arabinofuranosyltransferase (AftA) Involved in Cell Wall Arabinan Biosynthesis in *Mycobacterium tuberculosis*. *The Journal of biological chemistry* 281, 15653-15661.

Alderwick, L. J., Birch, H. L., Mishra, A. K., Eggeling, L. & Besra, G. S. (2007). Structure, function and biosynthesis of the *Mycobacterium tuberculosis* cell wall: arabinogalactan and lipoarabinomannan assembly with a view to discovering new drug targets. *Biochemical Society transactions* 35, 1325-1328.

Arnvig, K., Hove-Jensen, B. & Switzer, R. L. (1990). Purification and properties of phosphoribosyl-diphosphate synthetase from *Bacillus subtilis*. *European journal of biochemistry / FEBS* 192, 195-200.

Bald, D. & Koul, A. (2010). Respiratory ATP synthesis: the new generation of mycobacterial drug targets? *FEMS microbiology letters* 308, 1-7.

Banerjee, A., Dubnau, E., Quemard, A., Balasubramanian, V., Um, K. S., Wilson, T., Collins, D., de Lisle, G. & Jacobs, W. R., Jr. (1994). *inhA*, a gene encoding a target for isoniazid and ethionamide in *Mycobacterium tuberculosis*. *Science (New York, NY* 263, 227-230.

Barry, C. E., 3rd, Boshoff, H. I., Dartois, V., Dick, T., Ehrt, S., Flynn, J., Schnappinger, D., Wilkinson, R. J. & Young, D. (2009). The spectrum of latent tuberculosis: rethinking the biology and intervention strategies. *Nature reviews* 7, 845-855.

Bates, P. A., Kelley, L. A., MacCallum, R. M. & Sternberg, M. J. (2001). Enhancement of protein modeling by human intervention in applying the automatic programs 3D-JIGSAW and 3D-PSSM. *Proteins* Suppl 5, 39-46.

Becker, M. A., Smith, P. R., Taylor, W., Mustafi, R. & Switzer, R. L. (1995). The genetic and functional basis of purine nucleotide feedback-resistant phosphoribosylpyrophosphate synthetase superactivity, *J. Clin. Invest*. 96, 2133–2141.

Belanger, A. E., Besra, G. S., Ford, M. E., Mikusova, K., Belisle, J. T., Brennan, P. J. & Inamine, J. M. (1996). The *embAB* genes of *Mycobacterium avium* encode an arabinosyl transferase involved in cell wall arabinan biosynthesis that is the target for the antimycobacterial drug ethambutol. *Proceedings of the National Academy of Sciences of the United States of America* 93, 11919-11924.

Besra, G. S., Khoo, K. H., McNeil, M. R., Dell, A., Morris, H. R. & Brennan, P. J. (1995). A new interpretation of the structure of the mycolyl-arabinogalactan complex of *Mycobacterium tuberculosis* as revealed through characterization of oligoglycosylalditol fragments by fast-atom bombardment mass spectrometry and ^{1}H nuclear magnetic resonance spectroscopy. *Biochemistry* 34, 4257-4266.

Besra, G. S., Morehouse, C. B., Rittner, C. M., Waechter, C. J. & Brennan, P. J. (1997). Biosynthesis of mycobacterial lipoarabinomannan. *The Journal of biological chemistry* 272, 18460-18466.

Birch, H. L., Alderwick, L. J., Bhatt, A. & other authors (2008). Biosynthesis of mycobacterial arabinogalactan: identification of a novel $\alpha(1\rightarrow3)$ arabinofuranosyltransferase. *Molecular microbiology* 69, 1191-1206.

Boss, G. R., Idriss, S. D., Willis, R. C. & Seegmiller, J. E. (1984). Synthesis of (^{14}C)-ribose-5-phosphate and (^{14}C)-phosphoribosylpyrophosphate and their use in new enzyme assays. *Adv Exp Med Biol* 165 Pt B, 11-13.

Braven, J., Hardwell, T. R., Seddon, R. & Whittaker, M. (1984). A spectrophotometric assay of phosphoribosyl pyrophosphate synthetase. *Ann Clin Biochem* 21 (Pt 5), 366-371.

Briken, V., Porcelli, S. A., Besra, G. S. & Kremer, L. (2004). Mycobacterial lipoarabinomannan and related lipoglycans: from biogenesis to modulation of the immune response. *Molecular microbiology* 53, 391-403.

Carter, A. T., Beiche, F., Hove-Jensen, B., Narbad, A., Barker, P. J., Schweizer, L. M. & Schweizer, M. (1997). PRS1 is a key member of the gene family encoding phosphoribosylpyrophosphate synthetase in *Saccharomyces cerevisiae*. *Mol Gen Genet* 254, 148-156.

Cole, S. T. & Barrell, B. G. (1998). Analysis of the genome of *Mycobacterium tuberculosis* H37Rv. *Novartis Found Symp* 217, 160-172; discussion 172-167.

Combet, C., Jambon, M., Deleage, G. & Geourjon, C. (2002). Geno3D: automatic comparative molecular modelling of protein. *Bioinformatics* 18, 213-214.

Daffé, M., Brennan, P. J. & McNeil, M. (1990). Predominant structural features of the cell wall arabinogalactan of *Mycobacterium tuberculosis* as revealed through characterization of oligoglycosyl alditol fragments by gas chromatography/mass

spectrometry and by ^{1}H and ^{13}C NMR analyses. *The Journal of biological chemistry* 265, 6734-6743.

Dye, C. (2006). Global epidemiology of tuberculosis. *Lancet* 367, 938-940.

Eriksen, T. A., Kadziola, A., Bentsen, A. K., Harlow, K. W. & Larsen, S. (2000). Structural basis for the function of *Bacillus subtilis* phosphoribosyl-pyrophosphate synthetase. *Nature structural biology* 7, 303-308.

Fry, D. W., Becker, M. A. & Switzer, R. L. (1995). Inhibition of human 5-phosphoribosyl-1-pyrophosphate synthetase by 4-amino-8-(β-D-ribofuranosylamino)-pyrimido[5,4-d]pyrimidine-5'-monophosphate: evidence for interaction at the ADP allosteric site. *Molecular Pharmacology* 47, 810-815.

Gande, R., Gibson, K. J., Brown, A. K. & other authors (2004). Acyl-CoA carboxylases (accD2 and accD3), together with a unique polyketide synthase (*Cg-pks*), are key to mycolic acid biosynthesis in *Corynebacterianeae* such as *Corynebacterium glutamicum* and *Mycobacterium tuberculosis*. *The Journal of biological chemistry* 279, 44847-44857.

Gibson, K. J., Schubert, K. R. & Switzer, R. L. (1982). Binding of the substrates and the allosteric inhibitor adenosine 5'-diphosphate to phosphoribosylpyrophosphate synthetase from *Salmonella typhimurium*. *The Journal of biological chemistry* 257, 2391-2396.

Gibson, K. J., Eggeling, L., Maughan, W. N., Krumbach, K., Gurcha, S. S., Nigou, J., Puzo, G., Sahm, H. & Besra, G. S. (2003). Disruption of *Cg-Ppm1*, a polyprenyl monophosphomannose synthase, and the generation of lipoglycan-less mutants in *Corynebacterium glutamicum*. *The Journal of biological chemistry* 278, 40842-40850.

Hove-Jensen, B. (1985). Cloning and characterization of the *prs* gene encoding phosphoribosylpyrophosphate synthetase of *Escherichia coli*. *Mol Gen Genet* 201, 269-276.

Hove-Jensen, B. (1988). Mutation in the phosphoribosylpyrophosphate synthetase gene (*prs*) that results in simultaneous requirements for purine and pyrimidine nucleosides, nicotinamide nucleotide, histidine, and tryptophan in *Escherichia coli*. *Journal of bacteriology* 170, 1148-1152.

Hove-Jensen, B. (1989). Phosphoribosylpyrophosphate (PRPP)-less mutants of *Escherichia coli*. *Molecular microbiology* 3, 1487-1492.

Huang, H., Scherman, M. S., D'Haeze, W., Vereecke, D., Holsters, M., Crick, D. C. & McNeil, M. R. (2005). Identification and active expression of the *Mycobacterium tuberculosis* gene encoding 5-phospho-α-D-ribose-1-diphosphate: decaprenyl-phosphate 5-phosphoribosyltransferase, the first enzyme committed to decaprenylphosphoryl-d-arabinose synthesis. *The Journal of biological chemistry* 280, 24539-24543.

Koul, A., Dendouga, N., Vergauwen, K. & other authors (2007). Diarylquinolines target subunit c of mycobacterial ATP synthase. *Nat Chem Biol* 3, 323-324.

Koul, A., Vranckx, L., Dendouga, N. & other authors (2008). Diarylquinolines are bactericidal for dormant mycobacteria as a result of disturbed ATP homeostasis. *The Journal of biological chemistry* 283, 25273-25280.

Krath, B. N. & Hove-Jensen, B. (1999). Organellar and cytosolic localization of four phosphoribosyl diphosphate synthase isozymes in spinach. *Plant Physiol* 119, 497-506.

Lee, R. E., Brennan, P. J. & Besra, G. S. (1997). Mycobacterial arabinan biosynthesis: the use of synthetic arabinoside acceptors in the development of an arabinosyl transfer assay. *Glycobiology* 7, 1121-1128.

Li, S., Lu, Y., Peng, B. & Ding, J. (2007). Crystal structure of human phosphoribosylpyrophosphate synthetase 1 reveals a novel allosteric site. *The Biochemical journal* 401, 39-47.

Liu, H., Peng, X., Zhao, F., Zhang, G., Tao, Y., Luo, Z., Li, Y., Teng, M., Li, X. & Wei, S. (2009). N114S mutation causes loss of ATP-induced aggregation of human phosphoribosylpyrophosphate synthetase 1. *Biochel and Biophys Res Comm*. 379, 1120-1125

Madariaga, M. G., Lalloo, U. G. & Swindells, S. (2008). Extensively drug-resistant tuberculosis. *Am J Med* 121, 835-844.

Makarov, V., Manina, G., Mikusova, K. & other authors (2009). Benzothiazinones kill *Mycobacterium tuberculosis* by blocking arabinan synthesis. *Science (New York, NY* 324, 801-804.

McNeil, M., Daffe, M. & Brennan, P. J. (1991). Location of the mycolyl ester substituents in the cell walls of mycobacteria. *The Journal of biological chemistry* 266, 13217-13223.

Mikusova, K., Huang, H., Yagi, T. & other authors (2005). Decaprenylphosphoryl arabinofuranose, the donor of the D-arabinofuranosyl residues of mycobacterial arabinan, is formed *via* a two-step epimerization of decaprenylphosphoryl ribose. *Journal of bacteriology* 187, 8020-8025.

Ortalo-Magne, A., Dupont, M. A., Lemassu, A., Andersen, A. B., Gounon, P. & Daffe, M. (1995). Molecular composition of the outermost capsular material of the tubercle bacillus. *Microbiology (Reading, England)* 141 (Pt 7), 1609-1620.

Parry, R. J., Burns, M. R., Skae, P. N., Hoyt, J. C. & Pal, B. (1996). Carbocyclic analogues of D-Ribose-5-phosphate: Synthesis and behavior with 5-phosphoribosyl α-1-pyrophosphate synthetase. *Bioorgan & Med. Chem.* 4(7), 1077-1068.

Rao, S. P., Alonso, S., Rand, L., Dick, T. & Pethe, K. (2008). The protonmotive force is required for maintaining ATP homeostasis and viability of hypoxic, nonreplicating *Mycobacterium tuberculosis*. *Proceedings of the National Academy of Sciences of the United States of America* 105, 11945-11950.

Sassetti, C. M., Boyd, D. H. & Rubin, E. J. (2003). Genes required for mycobacterial growth defined by high density mutagenesis. *Molecular microbiology* 48, 77-84.

Schafer, A., Tauch, A., Jager, W., Kalinowski, J., Thierbach, G. & Puhler, A. (1994). Small mobilizable multi-purpose cloning vectors derived from the *Escherichia coli* plasmids pK18 and pK19: selection of defined deletions in the chromosome of *Corynebacterium glutamicum*. *Gene* 145, 69-73.

Scherman, M., Weston, A., Duncan, K., Whittington, A., Upton, R., Deng, L., Comber, R., Friedrich, J. D. & McNeil, M. (1995). Biosynthetic origin of mycobacterial cell wall arabinosyl residues. *Journal of bacteriology* 177, 7125-7130.

Scherman, M. S., Kalbe-Bournonville, L., Bush, D., Xin, Y., Deng, L. & McNeil, M. (1996). Polyprenylphosphate-pentoses in mycobacteria are synthesized from 5-phosphoribose pyrophosphate. *The Journal of biological chemistry* 271, 29652-29658.

Schubert, K. R., Switzer, R. L. & Shelton, E. (1975). Studies of the quaternary structure and the chemical properties of phosphoribosylpyrophosphate synthetase from *Salmonella typhimurium*. *The Journal of biological chemistry* 250, 7492-7500.

Schuck, P. (2004). A model for sedimentation in inhomogeneous media. I. Dynamic density gradients from sedimenting co-solutes. *Biophys Chem* 108, 187-200.

Schwede, T., Kopp, J., Guex, N. & Peitsch, M. C. (2003). SWISS-MODEL: An automated protein homology-modeling server. *Nucleic acids research* 31, 3381-3385.

Seidel, M., Alderwick, L. J., Birch, H. L., Sahm, H., Eggeling, L. & Besra, G. S. (2007). Identification of a Novel Arabinofuranosyltransferase AftB Involved in a Terminal Step of Cell Wall Arabinan Biosynthesis in *Corynebacterianeae*, such as *Corynebacterium glutamicum* and *Mycobacterium tuberculosis*. *The Journal of biological chemistry* 282, 14729-14740.

Stankiewicz, P. J. & Gresser, M. J. (1988). Inhibition of phosphatase and sulfatase by transition-state analogues. *Biochemistry* 27, 206-212.

Switzer, R. L. & Sogin, D. C. (1973). Regulation and mechanism of phosphoribosylpyrophosphate synthetase. V. Inhibition by end products and regulation by adenosine diphosphate. *The Journal of biological chemistry* 248, 1063-1073.

Tozzi, M. G., Camici, M., Mascia, L., Sgarrella, F. & Ipata, P. L. (2006). Pentose phosphates in nucleoside interconversion and catabolism. *Febs J* 273, 1089-1101.

Turnock, D. C. & Ferguson, M. A. (2007). Sugar nucleotide pools of *Trypanosoma brucei*, *Trypanosoma cruzi*, and *Leishmania major*. *Eukaryot Cell* 6, 1450-1463.

Wayne, L. G. & Sohaskey, C. D. (2001). Nonreplicating persistence of *Mycobacterium tuberculosis*. *Annu Rev Microbiol* 55, 139-163.

Willemoes, M., Hove-Jensen, B. & Larsen, S. (2000). Steady state kinetic model for the binding of substrates and allosteric effectors to *Escherichia coli* phosphoribosyl-diphosphate synthase. *The Journal of biological chemistry* 275, 35408-35412.

Wojtkiewicz, B., Szmidzinski, R., Jezierska, A. & Cocito, C. (1988). Identification of a salvage pathway for D-arabinose in *Mycobacterium smegmatis*. *European journal of biochemistry / FEBS* 172, 197-203.

Wolucka, B. A., McNeil, M. R., de Hoffmann, E., Chojnacki, T. & Brennan, P. J. (1994). Recognition of the lipid intermediate for arabinogalactan/arabinomannan biosynthesis and its relation to the mode of action of ethambutol on mycobacteria. *The Journal of biological chemistry* 269, 23328-23335.

Figure Legends

Figure 1. Proposed metabolic pathway depicting the importance of Mt-PrsA for the generation of pRpp in *M. tuberculosis*. R5P is generated *via* the catabolism of glucose through the pentose phosphate pathway, a process ubiquitous throughout nature. Like all pRpp synthetase enzymes, Mt-PrsA catalyses the transfer of pyrophosphate from ATP to the C1-OH group of R5P forming pRpp and AMP. In a process unique to members belonging to the *Corynebacteriaceae*, such as *M. tuberculosis*, pRpp is utilised as the sole metabolic intermediate in the formation of DPA, which is a crucial substrate required for mycobacterial cell wall assembly. (DP) decaprenol-1-monophosphate, (DPA) decaprenol-1-monophosphoarabinose, (DPR) decaprenol-1-monophosphoribose, (DPPR) decaprenol-1-monophosphoribose-5-phosphate, (DPX) decaprenol-1-monophosphoryl-2-keto-β-*erythro*-pentofuranose, (pRpp) phosphoribosyl-1-pyrophosphate, (R5P) ribose -5-phosphate.

Figure 2. Time course assay showing Mt-PrsA catalysed formation of p[^{14}C]Rpp from [^{14}C]R5P and ATP. Assays contained Mt-PrsA, 50 mM Pi, 2mM ATP supplemented with either 2 mM Mg^{2+}, Mn^{2+} or Ca^{2+} as illustrated in panel ***A***, and in the presence of ADP at a final concentration of 2 mM in panel ***B***. Assays were incubated at 37 °C and aliqouts were removed from the assay mix at 0, 10, 30 and 60 seconds and the reactions halted by quenching with addition of formic acid. Samples were applied to a glass-backed PEI-cellulose TLC plate and developed in 0.85 M KH_2PO_4 (pH 3.4). The

plate was inspected for radioactive spots relating to p[^{14}C]Rpp and [^{14}C]R5P by autoradiography through the exposure of TLCs to X-ray film (Kodak X-Omat).

Figure 3. Analysis of Mt-PrsA dependent [^{14}C]-R5P incorporation into the *M. smegmatis* arabinofuranosyltransferse substrate DPA *via* p[^{14}C]Rpp. The basic assays mixture contained (amongst other components described in materials and methods) membranes prepared from *M. smegmatis*, 100,000 cpm [^{14}C]-R5P, 50 μg DP and 2 mM ATP. Individual assays were carried out at 37 °C and included the addition of no further additive, lane 1, *M. smegmatis* P60, lane 2, Mt-PrsA, lane 3, Mt-PrsA and $NaWO_4$ and NaF both at a final concentration of 2 mM, lane 4, Mt-PrsA and *M. smegmatis* P60, lane 5, Mt-PrsA, *M. smegmatis* P60 and 2 mM of both $NaWO_4$ and NaF, lane 6 and finally Mt-PrsA, *M. smegmatis* P60 and 2 mM ADP in lane 7. After an inubation at 37 °C for 30 min, assays were quenched and products extracted from the assay mix by organic solvent extraction as described in materials and methods. Samples relating to each assay were loaded onto a silica gel TLC plates, developed in $CHCl_3/CH_3OH/CH_3COONH_4/NH_4OH/H_2O$ (180:140:9:9:23 v/v/v/v/v) and bands migrating to the position of DPA, DPR, DPX and DPPR were visualised by autoradiography, exposure of TLCs to X-ray film (Kodak X-Omat) and compared to previously isolated known standards (Mikusova *et al.*, 2005; Alderwick *et al.*, 2006a).

Figure 4. Arabinofuranosyltransferase assays carried out *via* the Mt-PrsA-dependent conversion of [^{14}C]-R5P to p[^{14}C]Rpp and subsequent chase into a neo-glycolipid acceptor. The absolute dependence of the cell wall AraT enzymes on the

availability of pRpp was investigated using the neo-glycolipid acceptor α-D-Ara*f*-(1→5)-α-D-Ara*f*-*O*-$(CH_2)_7CH_3$ (Ara_2). The basic assay contained (amongst other components described in materials and methods) 0.5 mg of membranes and P60 from *M. smegmatis*, 2 mM α-D-Ara*f*-(1→5)-α-D-Ara*f*-*O*-$(CH_2)_7CH_3$, 100,000 cpm [^{14}C]-R5P, 50 μg DP and 2 mM ATP. Assays were initiated by the addition of [^{14}C]-R5P and incubated for 1 hour at 37 °C. Individual assays carried out contained the addition of no Mt-PrsA, lane 1, 30 μg Mt-PrsA, lane 2, 30 μg Mt-PrsA and 100 μg/ml EMB, lane 3 and 30 μg Mt-PrsA and 2 mM ADP in lane 4. [^{14}C]-Ara*f*-linked products were extracted from the assay mix as described in materials and methods and subsequently applied to a silica gel TLC plates, developed in $CHCl_3$:CH_2OH:H_2O:NH_4OH (65:25:3.6:0.5, v/v/v/v) and visualised by autoradiography from exposure of TLCs to X-ray film (Kodak X-Omat) (Lee *et al.*, 1997; Seidel *et al.*, 2007).

Figure 5. Enzyme activity of Mt-PrsA and kinetic characterisation of R5P (A) and ATP (B) using a continuous enzyme coupled spectrophotometric assay. *A*, a plot of velocity (ν) of Mt-PrsA to increasing [R5P] in the presence of 50 mM Pi (●), 5 mM Pi (■) and no Pi (▲). Data for 50 mM Pi fitted to equation 2 and data, obtained for 5 mM Pi and no Pi were fitted to equation 3. *B*, a plot of velocity (ν) of Mt-PrsA to increasing [ATP] in the presence of 50 mM Pi (●), 5 mM Pi (■) and no Pi (▲), all of which were fitted to equation 4 using nonlinear regression analysis. All data points plotted (calculated mean) represent experiments performed in triplicate using three independent preparations of recombinant Mt-PrsA. Calculated standard errors (± Std. Errors) for kinetic constants are reported in the manuscript where appropriate.

Figure 6. Inhibition of Mt-PrsA activity by the addition of ADP when titrated with R5P (A) and ATP (B) using a continuous enzyme coupled spectrophotometric assay. A, a plot of velocity (ν) of Mt-PrsA response to increasing [R5P] in the presence of no ADP (●), 0.1 mM ADP (■) and 2 mM ADP (▲). Data was fitted to equation 5 using nonlinear regression analysis. A, a plot of velocity (ν) of Mt-PrsA response to increasing [ATP] in the presence of no ADP (●), 0.1 mM ADP (■) and 2 mM ADP (▲). Data was fitted to equation 6 using nonlinear regression analysis. All data points plotted (calculated mean) represent experiments performed in triplicate using three independent preparations of recombinant Mt-PrsA. Calculated standard errors (± Std. Errors) for kinetic constants are reported in the manuscript where appropriate.

Figure 7. Mt-PrsA self-assembly analysis using analytical ultracentrifugation. Sedimentation velocity experiments were conducted to investigate the oligomeric state of Mt-PrsA in solution in the presence of no additional ligands (black line), 5 mM R5P (red line), 5 mM ATP (blue line) and 5 mM ADP (green line). Individual plots represent the molar mass dristribution c(M) *vs* the apparent molecular weight (Da). Arrows indicate the calculated oligomeric state of Mt-PrsA in each sedimentation velocity experiment.

Figure 8. Binding kinetics of R5P (A) and the ATP analogue (AMPPNP) (B) to Mt-PrsA using Intrinsic Tryptophan Fluorescence Spectroscopy. Intrinsic tryptophan fluorescence spectroscopy was used to determine the binding properties of Mt-PrsA for its substrates R5P and ATP. Ligand binding assays were carried out as described in

materials and methods. *A*, a plot of $\Delta F_{emission}$ vs [R5P] in the presence of no AMPPNP (■) and 5 mM AMPPNP (●) which was fitted to equation 7. *B*, a plot of $\Delta F_{emission}$ vs [AMPPNP] in the presence of no R5P (■) and 5 mM R5P (●) which was fitted to equation 9.

Figure 9. Binding kinetics of ADP and the ATP to Mt-PrsA using Intrinsic Tryptophan Fluorescence Spectroscopy. Intrinsic tryptophan fluorescence spectroscopy was used to determine the binding properties of Mt-PrsA for it's the allosteric inhibitor ADP and in competition with ATP. Ligand binding assays were carried out as described in materials and methods. *A*, a plot of $\Delta F_{emission}$ vs [ADP] (●) which was fitted to equation 8. *B*, a plot of $\Delta F_{emission}$ vs [ATP] in the presence of no ADP (■), 0.1 mM ADP (▲) and 2.0 mM ADP (▼) which was fitted to equation 10.

Figure 10. Sequence alignment of various prokaryotic pRpp synthetases. Protein sequences from *M. tuberculosis* (Mt_PrsA), *M. smegmatis* (Ms_PrsA), *M. leprae* (Ml_PrsA), *C. glutamicum* (Cg_PrsA), *S. coleicolor* (Sc_Prs), *B. subtilis* (Bs_Prs), *E. coli* (Ec-Prs) and the three PrsA isoforms (Human_PrsA1-3) were aligned using CLUSTALW and annotated with ESPRIPT. Green triangles represent residues involved in catalysis. Blue circles indicate conserved and open blue circles highlight non-conserved residues involved in allosteric regulation. His109 and Gly111 are highlighted with red stars, indicating two residues only found in the flexible loop region of *Corynebacterianeae* PrsA homologues. The magenta diamonds indentify the location of the residues involved in the formation of a salt bridge in Bs-PrsA and Human-PrsA1.

Figure 11. Homology model of Mt-PrsA. *A*, Mt-PrsA arranged into its hexameric quaternary conformation. Carbon atoms of the ADP ligands located at the catalytic and regulatory sites of the Mt-PrsA hexamer are coloured in orange and green, respectively. Red spheres located at K10, D169, G194, D205-V208 and F322 indicate regions of the Mt-PrsA dimmer that include insertions or deletions with respect to the Bs-Prs structure. The triangle in the middle represents 3-fold symmetry, where as the arrow parallel to the plane indicates 2-fold rotational symmetry. Catalytic (*B*) and regulatory (*C*) sites of the Mt-PrsA homology model. The yellow and blue spheres indicate A85/G88 and S109/G111 substitution between the Bs-Prs and Mt-PrsA structures, respectively.

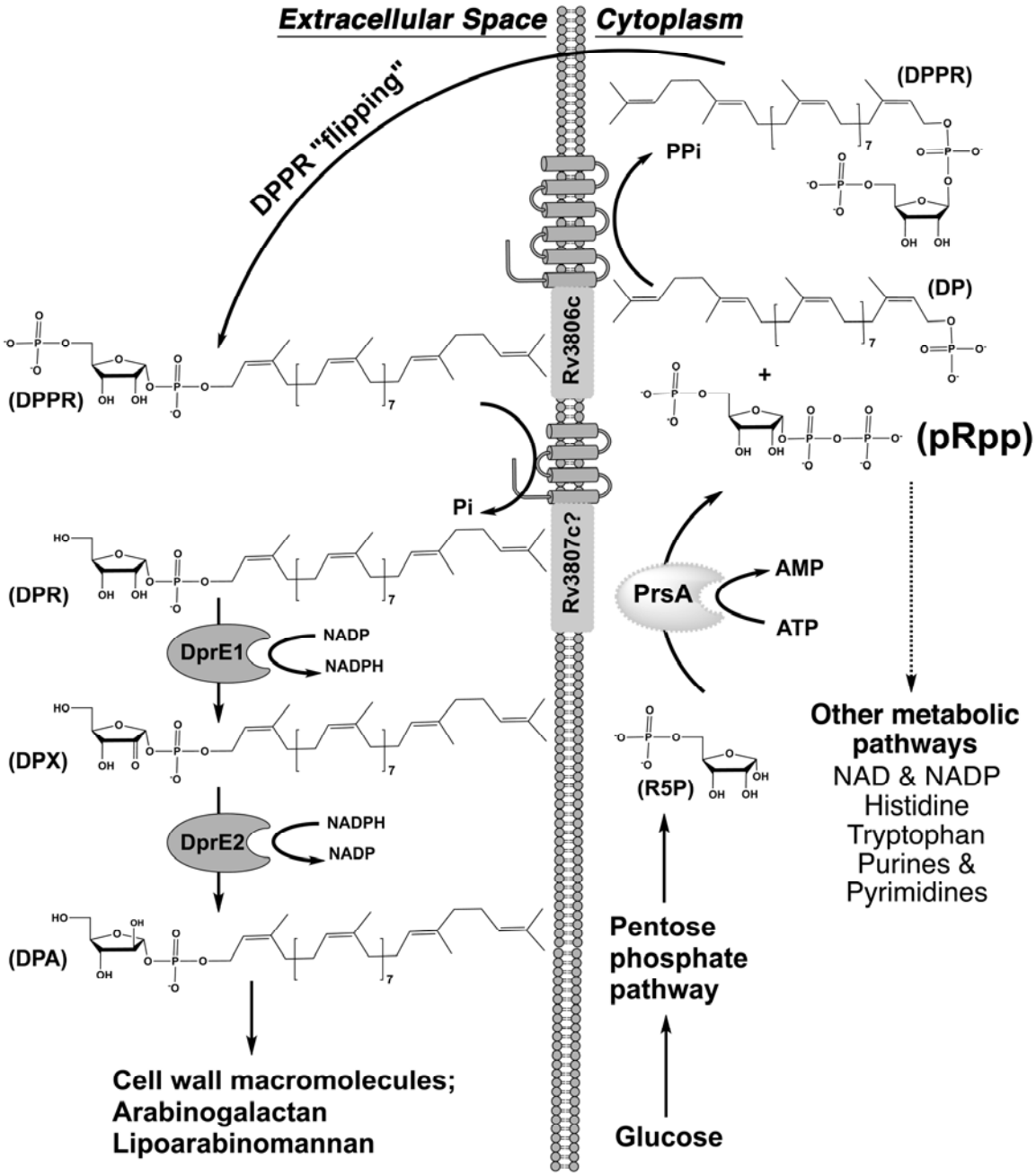

Fig. 1

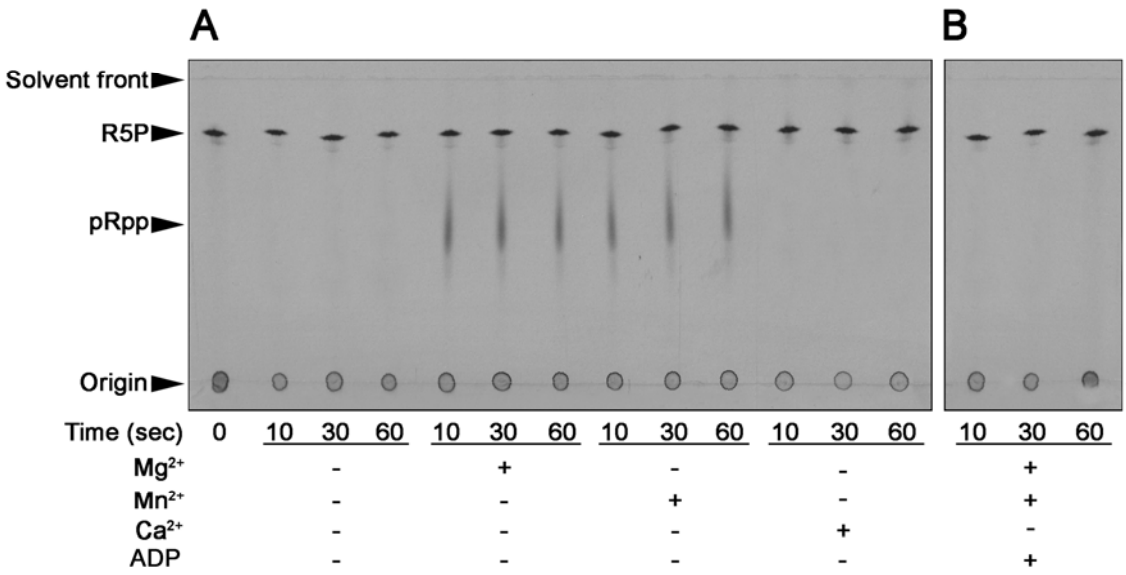

Fig. 2

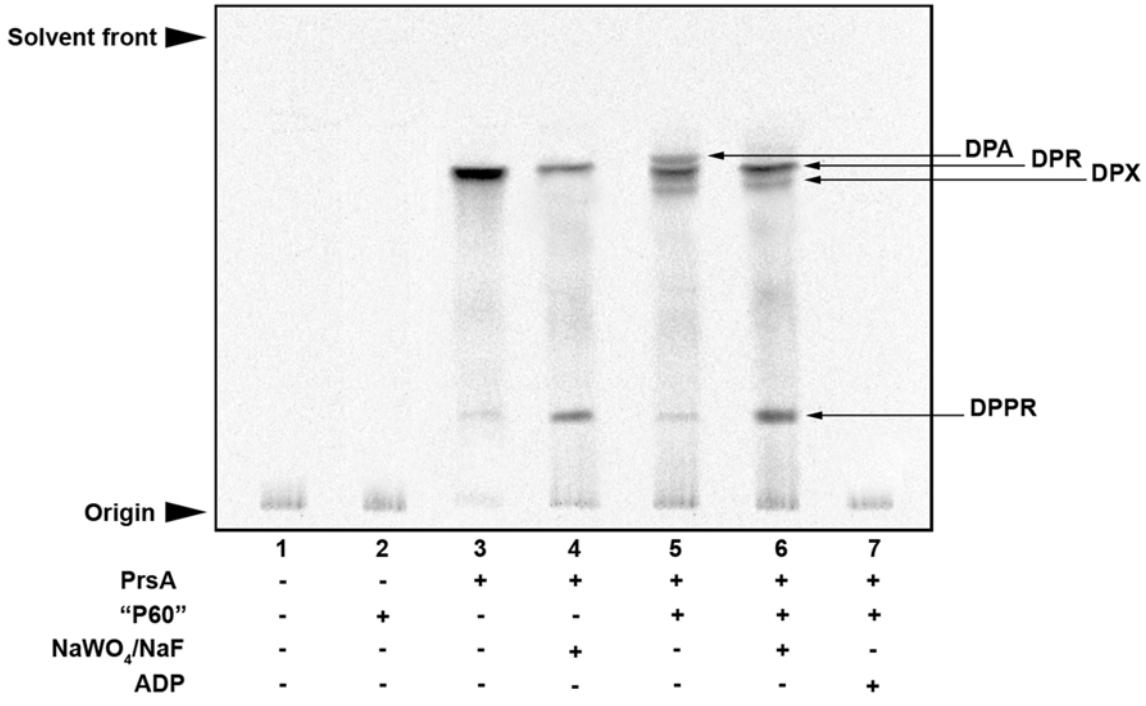

Fig. 3

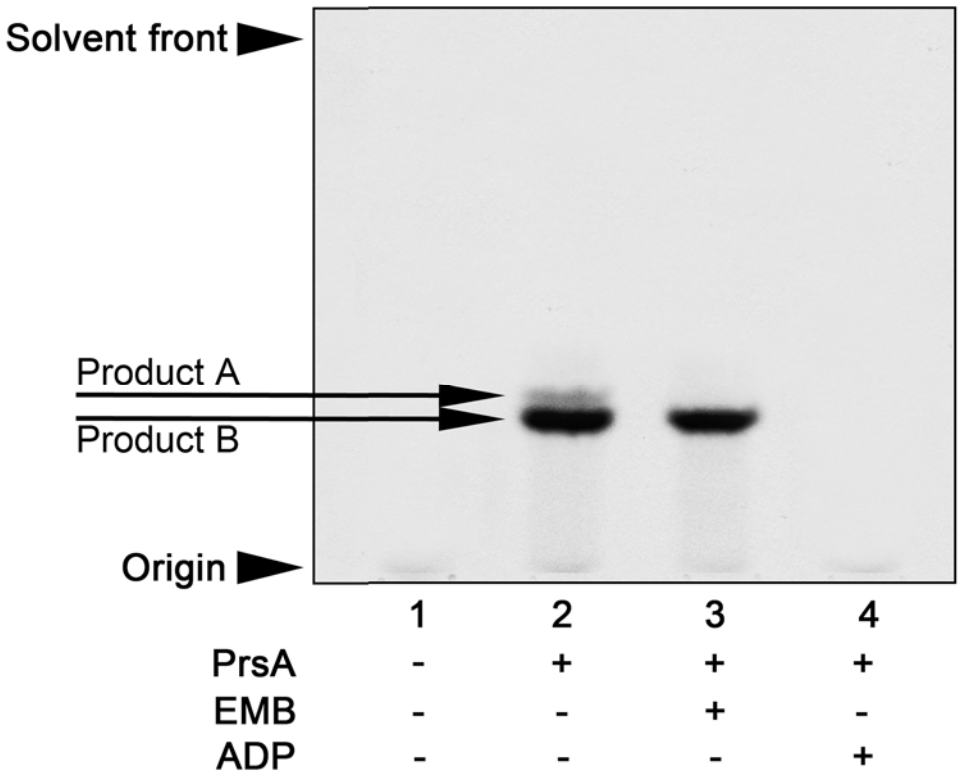

Fig. 4

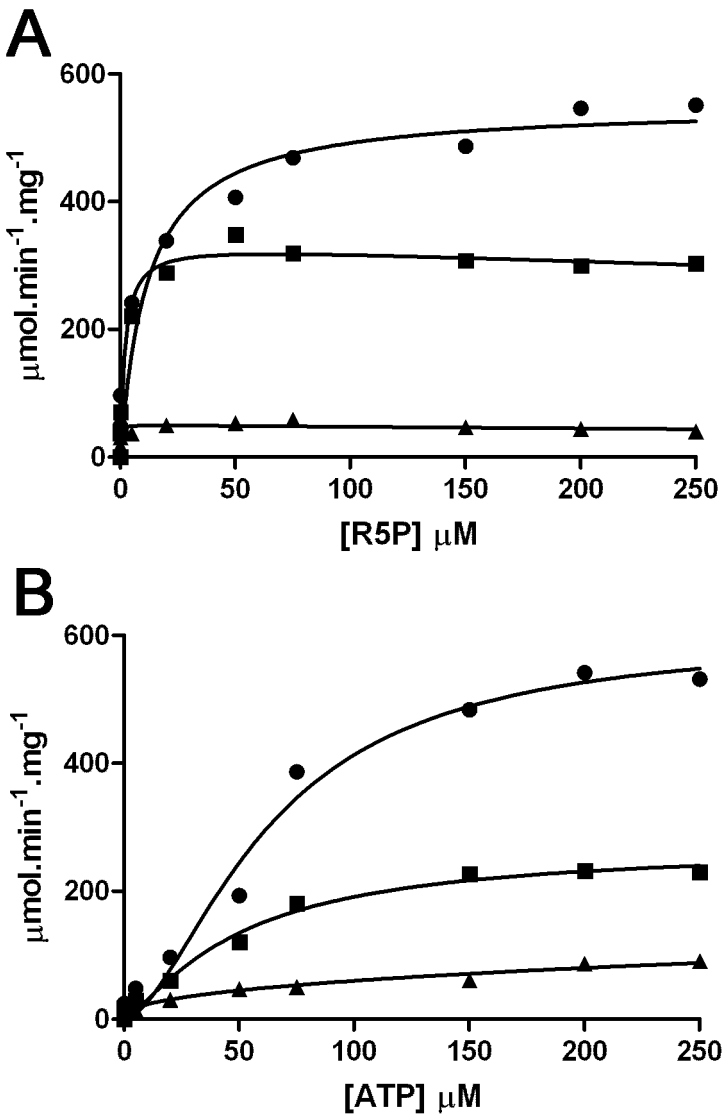

Fig. 5

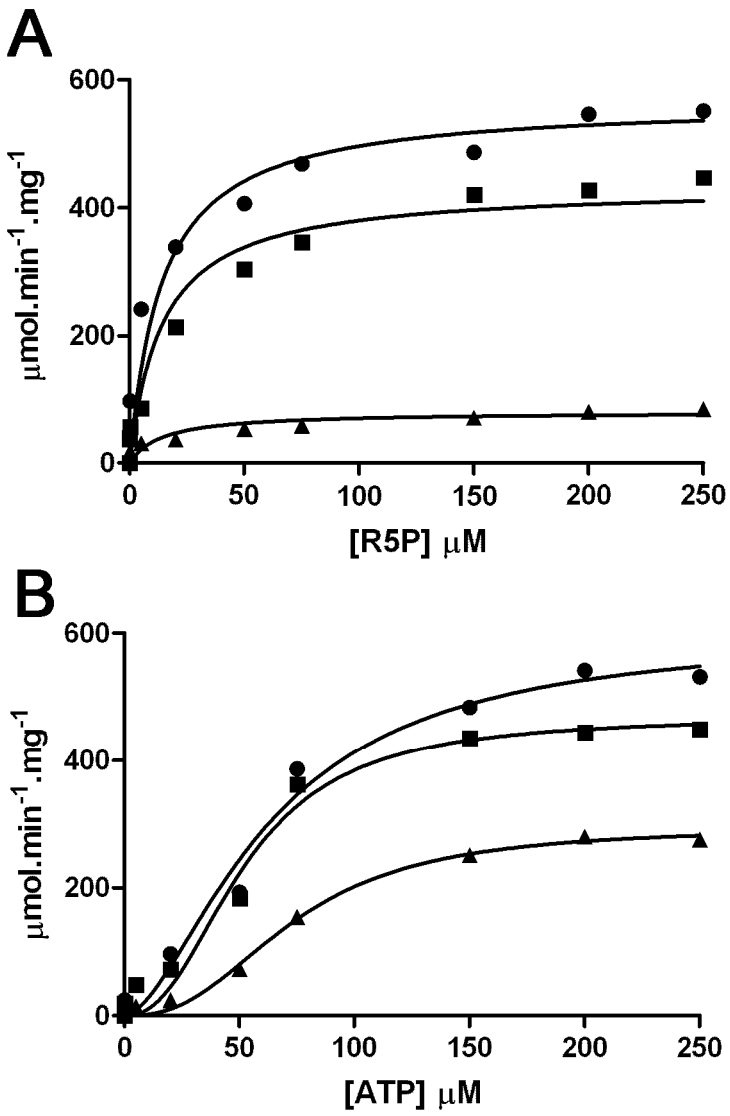

Fig. 6

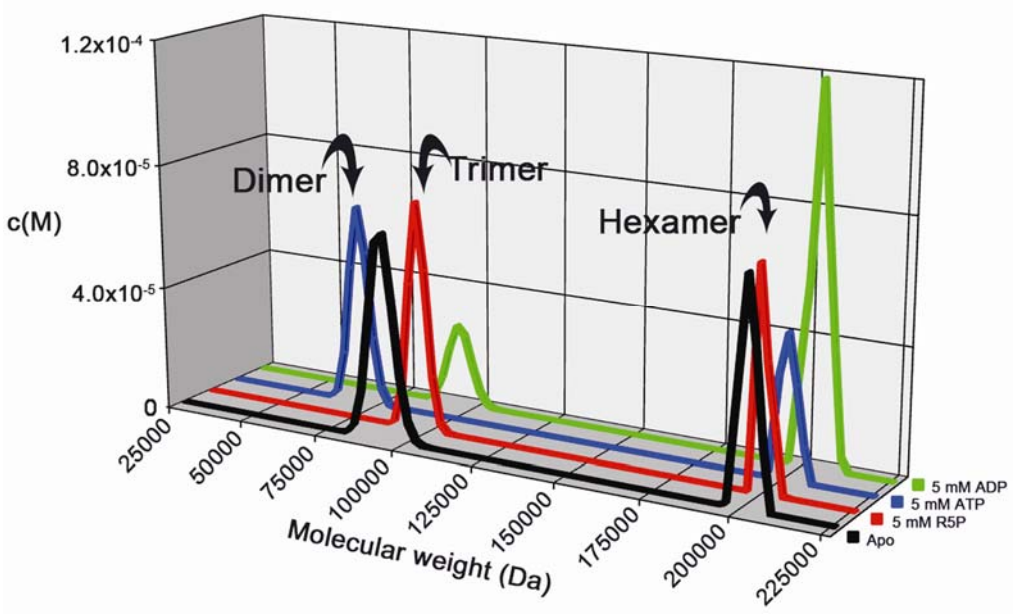

Fig. 7

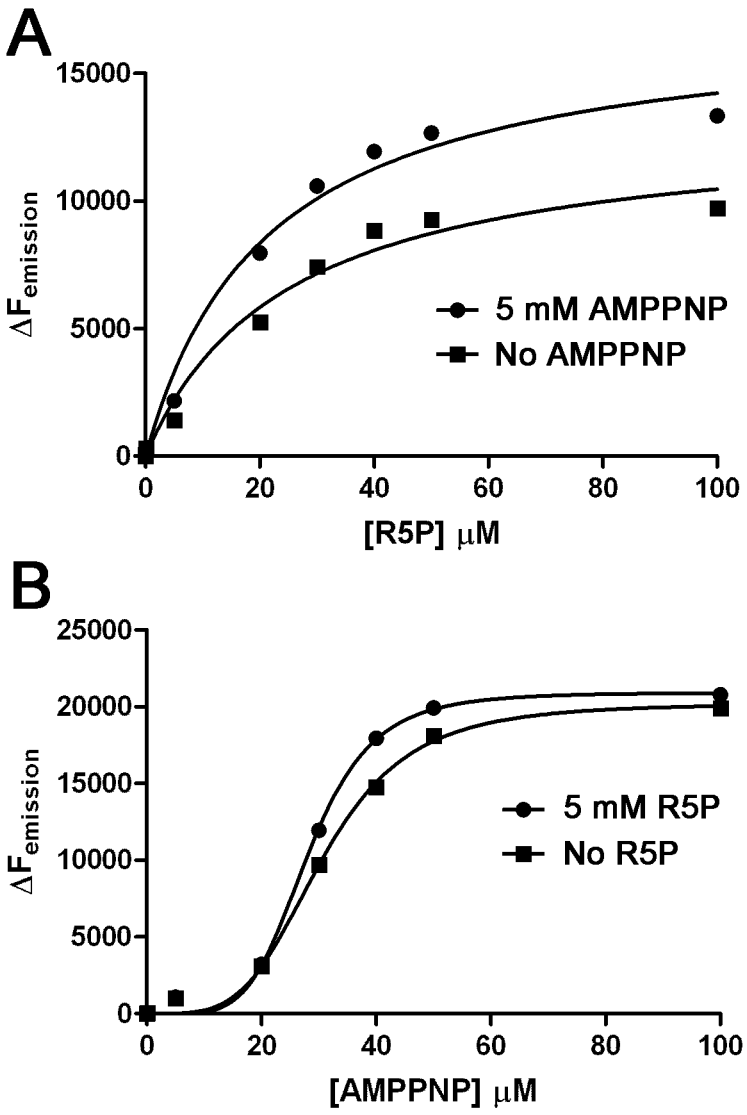

Fig. 8

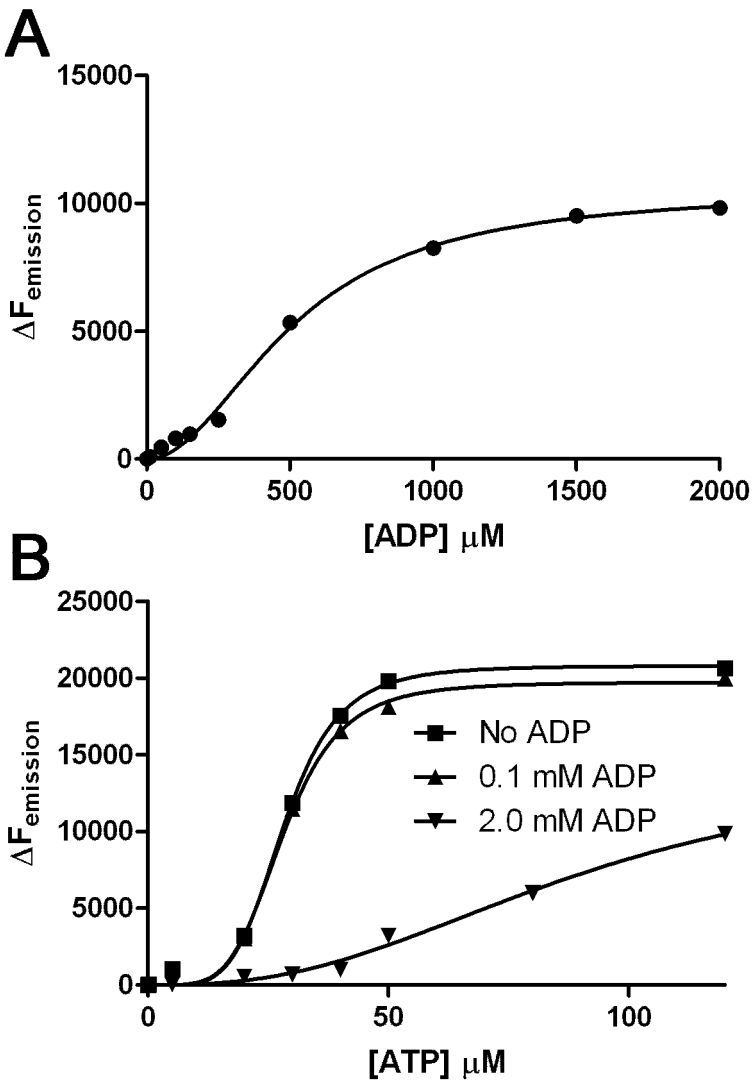

Fig. 9

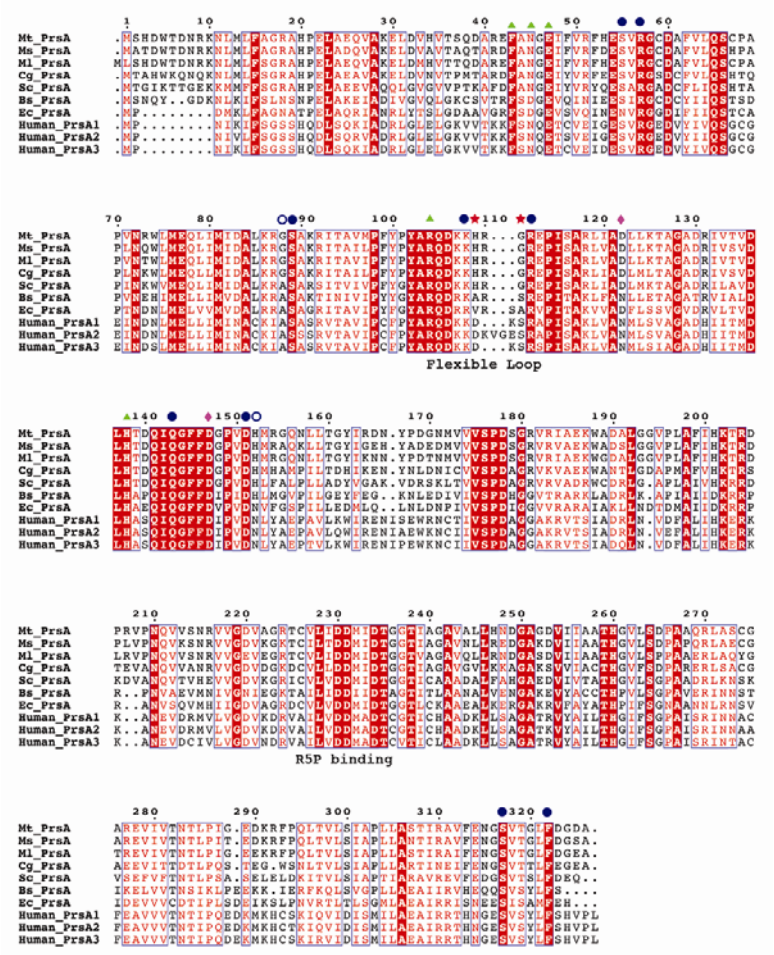

Fig. 10

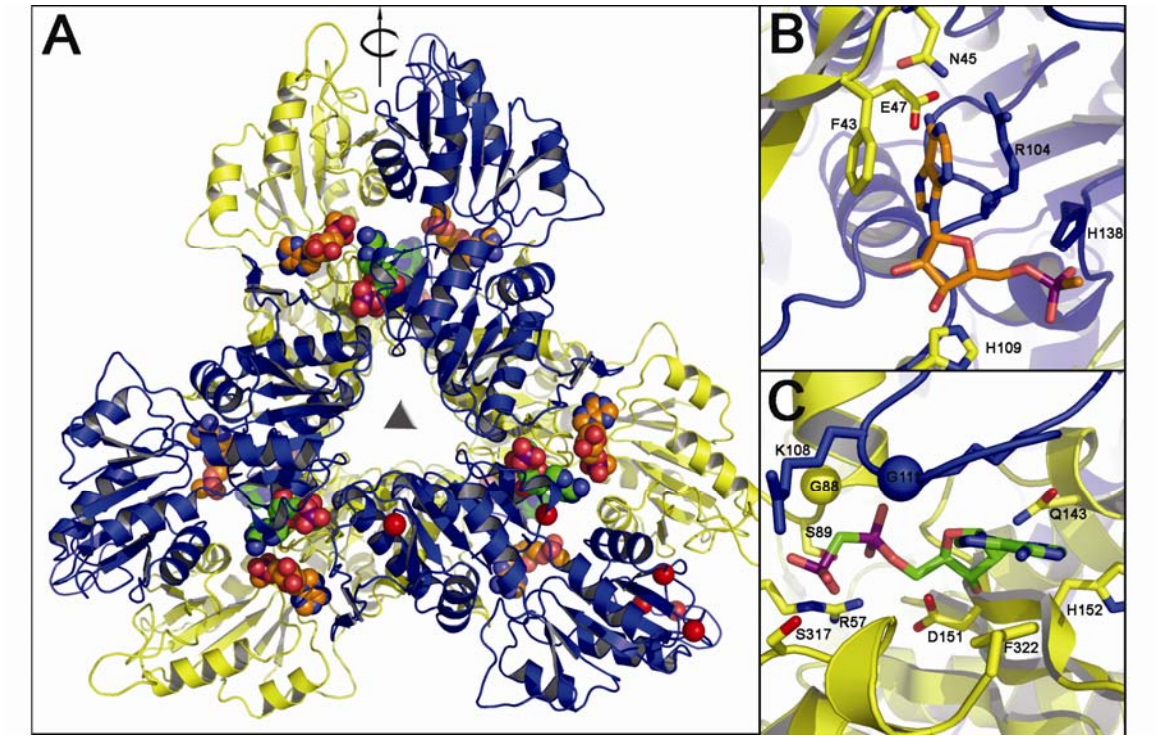

Fig. 11